Part IV

Norman West '99

Chapter 14

Borehole Density and Acoustic Velocity Measurements, Borehole N-033, Norman West

By **K.A. Pflug, C.J. Mwenifumbo, M. Salisbury and J. Hawken**

Introduction

The Borehole Geophysics and Petrophysics Section of the Geological Survey of Canada (GSC) conducted full waveform sonic and density measurements in borehole N-033 on the Norman West property of Falconbridge Ltd., near Sudbury, Ontario. The hole intersects granophyre, norite, breccia, gneiss and semi-massive Cu-Ni-sulphide mineralization. Spot measurements of acoustic velocity and density were conducted by GSC Atlantic on core samples representing all lithological units intersected in the borehole. The main objective of this program was to provide acoustic velocity and density data to the Downhole Seismic Imaging Consortium to aid in the interpretation of downhole seismic data.

Log Data Acquisition and Processing

The logs were acquired in December 1999, to a depth of 2100 m, with the GSC logging system using a Mount Sopris full waveform sonic probe (model CLP-4681) and a GSC-developed density probe. Data were acquired while logging downwards and upwards providing redundancy of data. Logging speeds were 9 m/minute for the density logs and the acoustic down-hole run, and 6 m/minute for the acoustic up-hole run. The sample depth intervals for these logging speeds are 15 cm and 10 cm, respectively, for a sample time interval of one second.

Sonic Logging

Probe Description and Data Acquisition Procedure

The sonic probe is 2.8 meters long, 45-mm diameter and consists of a single piezoelectric transducer transmitter, with a centre frequency of about 28 kHz, and two piezoelectric transducer receivers separated by about 30 cm. The transmitter-receiver spacings are 0.9 m and 1.2 m (3 ft and 4 ft). The transmitter pulses twice per second and the acoustic signal is digitized alternately by the two receivers for a period of about 1 millisecond at 4 microsecond intervals. The difference in the arrival time of the acoustic signal at the two receivers provides a measure of the P-wave velocity every second. The penetration of the acoustic energy depends on the seismic velocity of the rock. It is about 20 cm for P waves with this tool.

Density Logging

Probe Description and Data Acquisition Procedure

The GSC density probe is 1.2 m in length and 38 mm in diameter. It is a spectral gamma-gamma density logging probe with a weak, 10 millicurie (370 MBq), omnidirectional ^{60}Co gamma-ray source on it's nose. The probe has a single, 25 mm by

76 mm (1" x 3") cesium iodide detector which detects gamma rays from the source that are backscattered by the rock around the borehole. The detector is located 37 cm from the ^{60}Co source. Complete backscattered gamma-ray spectra are recorded every second in 1024 channels over an energy range of 0 to 800 keV. The penetration of back-scattered gamma rays is approximately 10 to 15 cm.

Density Log Calibration

The density is computed from the sum of counts in an energy window, 200-500 keV (W06). Detailed core density measurements from a portion of hole N-033 in the vicinity of the sulphide mineralization were provided by the Continental Geoscience Division (CGD) of the GSC to calibrate the probe at Norman West. These core densities were plotted with core densities from Bells Corners hole BC-81-2 (the deep-test hole normally used for calibrating the GSC's probes for NQ-size holes) against the W06 count rate (Fig. 1). Density versus count rate is non-linear over the measured density range (2 - 5 g/cm^3). A natural logarithmic transform gave a fairly good fit to the data and provided the following relationship: density = -2.226 x ln(W06) + 18.88. This equation was used to calibrate the density probe at Norman West. The regression from the calibration on the Bells Corners data only is shown in Figure 17.1 for comparison.

Core Density and Acoustic Velocity Measurements

The core density and P-wave velocity measurements performed by GSC Atlantic are presented in Table 14.1. Density measurements were made on whole core samples (6-8 inches long by 2.5 inches in diameter) and mini-core samples (1-2 inches long by 2.5 inches in diameter). P-wave velocity was measured on the mini-core samples at in-situ pressure and at 200 MPa.

Geophysical Logs

The density, P-wave velocity and acoustic impedance logs for hole N-033 are shown in Figure 17.2 along with the full waveform log from the far receiver. The velocity and density logs for hole N-033 were averaged over 1 metre intervals before the impedance was computed. A simplified lithology log, fracture log, and copper and nickel assays are also shown in Figure 17.2.

The density and P-wave velocity logs for hole N-033 are shown in Figure 17.3, with the lab core density (whole core) and P-wave velocity (at in-situ pressure) measurements overlain for comparison. The log data and core data agree fairly well. Discrepancies are likely due to the presence of fracturing in the borehole which produces lower in-situ densities and velocities than those measured on solid core, as well as depth

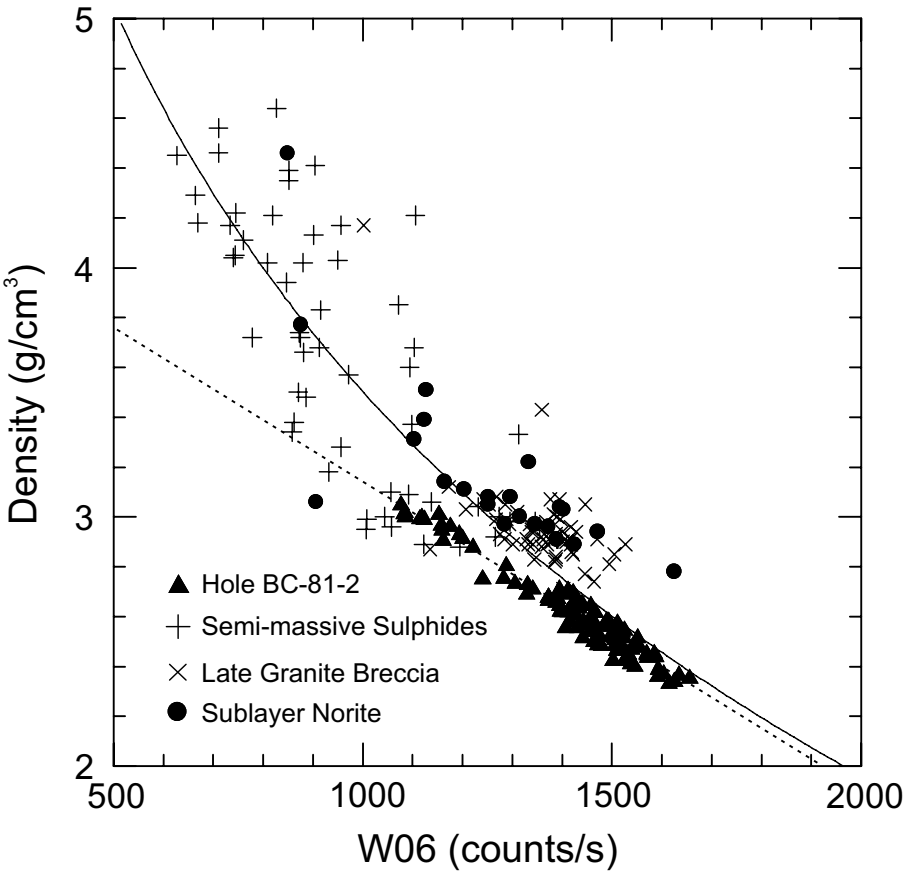

Figure 14.1: Core density versus count rate in the energy window W06 (200-500 keV) from the density probe, holes N-033 and BC- 81-2. The solid line (density = -2.226 x ln(W06) + 18.88) is the natural logarithmic fit used to calibrate the density probe at Norman West. The dashed line (density = -0.00124 x W06 + 4.38) is the regression from BC-81-2 only and is provided for reference.

mismatch and sample-size differences between the log data and core samples. A Z/A (atomic number over atomic weight) correction factor was not applied to the density data and this would account for some of the discrepancy.

Average densities, velocities and impedances computed from the log data for the different (simplified) lithologies are presented in Table 14.2. The highly fractured, low-density interval from 1621.5-1640.1 m in the sublayer norite was excluded from the averages. The Cu-Ni-sulphide mineralization is characterized by higher densities (3.52 g/cm^3), lower velocities (5.72 km/s) and higher impedances (20.02 km/s g/cm^3) than the host rocks ($<$ 3 g/cm^3, $>$6 km/s and $<$ 19 km/s g/cm^3, respectively). From the values in Table 14.2, a reflection coefficient of 0.055 is predicted for the late granite breccia/semi-massive sulphide contact.

Rock Type	Depth (m)	Whole Core Density (g/cm^3)	Mini-Core Density (g/cm^3)	Vp @ in-situ pressure (km/s)	Vp @ 200 MPa (km/s)
Granophyre	372	2.79	2.68	5.70	6.32
Granophyre transition	621	2.79	2.83	5.97	6.27
Felsic norite	942	2.82	2.83	6.23	6.58
Felsic norite	1239	2.81	2.81	6.15	6.45
Mafic norite	1420	2.77	2.72	5.69	5.88
Sublayer norite	1459	2.93	2.89	6.16	6.46
Norite breccia	1554	3.20	3.20	6.70	6.99
Norite breccia	1617	3.00	2.95	6.32	6.69
Ultramafic	1625	2.82	2.76	6.17	6.36
Basalt	1672	2.97	3.00	6.40	6.66
Gabbro	1686	3.13	2.90	6.28	6.51
Gabbro	1692	2.85	2.84	5.82	6.07
Massive Po,Bo,(Cpy)	1701	4.44	4.49	4.80	5.00
Semi-massive Po,Bo,Cpy	1718	3.94	4.22	5.30	5.44
Massive Po,Cpy,Bo	1729	4.19	4.51	4.84	4.98
Diabase	1859	2.99	2.97	6.37	6.59
Sudbury breccia	1954	2.74	2.74	5.97	6.15
Intermediate gneiss	2052	2.76	2.76	6.03	6.29
Sudbury breccia	2077	2.76	2.77	6.04	6.25
Felsic gneiss	2117	2.66	2.66	5.87	6.21

Table 14.1: Spot core density and P-wave velocity (Vp) measurements for the different lithologies intersected in borehole N-033.

Rock Type	Depth Interval (m)	Density (g/cm^3)		Vp (km/s)		Impedance (km/s g/cm^3)	
		Mean	Std. Dev.	Mean	Std. Dev.	Mean	Std. Dev.
Granophyre	45 - 584	2.65	0.06	6.02	0.12	15.95	0.56
Transition Zone	584 – 870.4	2.91	0.10	6.42	0.14	18.67	0.90
Felsic Norite	870.4 - 1454	2.70	0.07	6.33	0.14	17.13	0.75
Sublayer Norite	1454 – 1659.3	3.00	0.19	6.17	0.26	18.54	1.26
Late Granite Breccia	1659.3 – 1699.6 1735.21 – 1924.51	2.79	0.14	6.42	0.21	17.93	1.28
Semi-Massive Sulphides	1699.6 – 1735.21	3.52	0.40	5.72	0.43	20.02	1.45
Sudbury Breccia	1924.51- 2037 2065.5 - 2095	2.75	0.13	6.28	0.22	17.28	1.33
Intermediate Gneiss	2037 – 2065.5	2.65	0.06	6.31	0.09	16.74	0.52

Table 14.2: Means and standard deviations for density, P-wave velocity (Vp) and acoustic impedance, computed from the logs, for the different (simplified) lithologies intersected in borehole N-033.

Acknowledgement

The authors wish to thank Bill Hyatt and Jacques Parker for acquiring the density and acoustic logs and Erick Adam for providing the core density measurements used to calibrate the density probe.

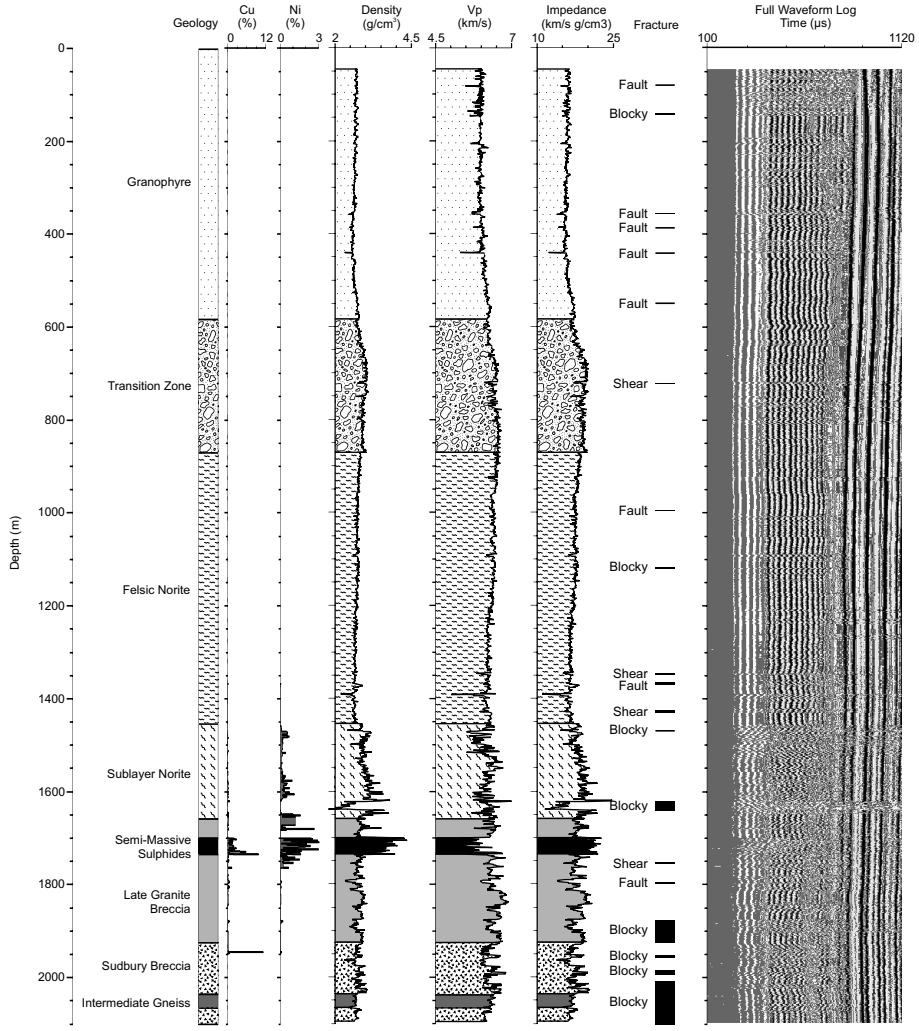

Figure 14.2: Density, P-wave velocity (Vp), acoustic impedance and full waveform logs for borehole N-033, shown with the geology, Cu assay, Ni assay and fracture logs.

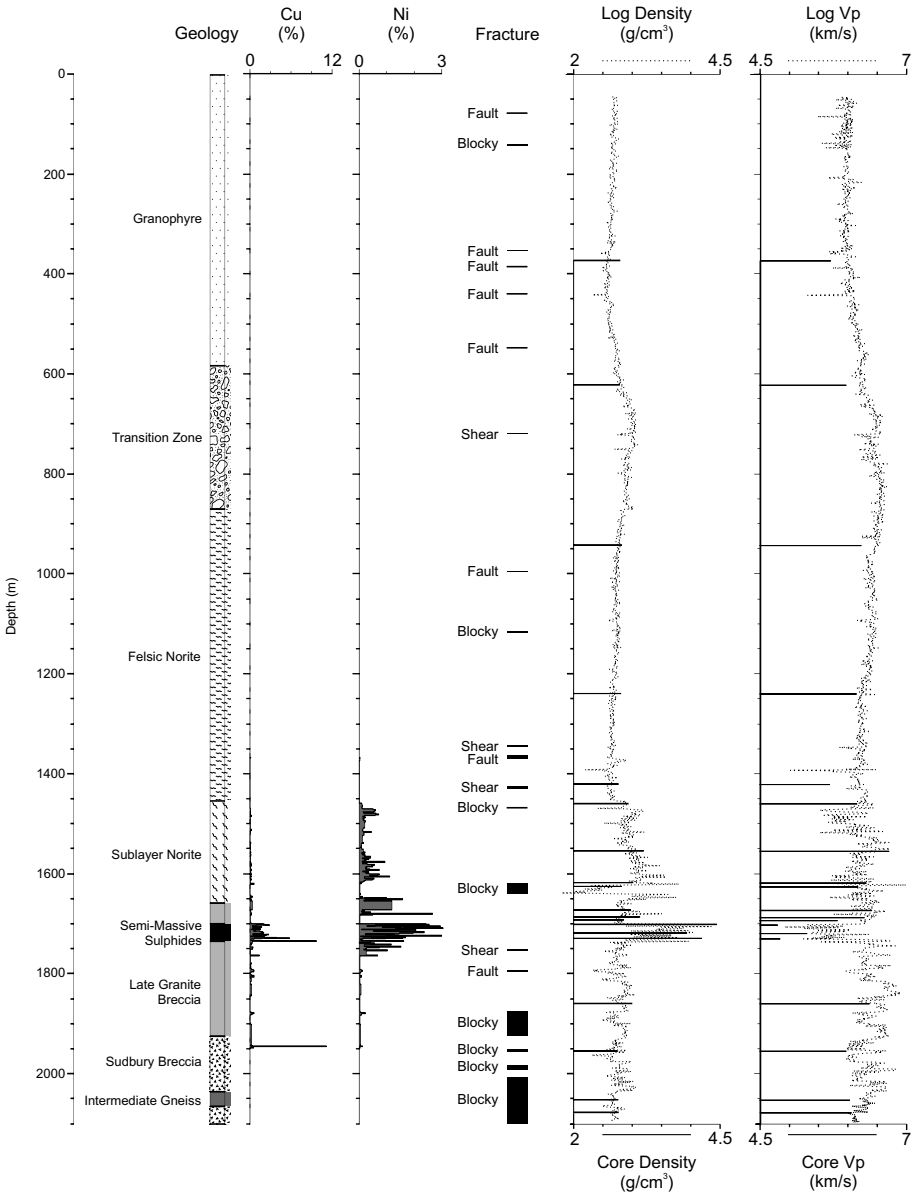

Figure 14.3: Comparison of log density and P-wave velocity (Vp) measurements with GSC Atlantic core density (whole core) and P-wave velocity (at in-situ pressure) measurements.

Chapter 15

Acquisition at Norman West 99, Sudbury, Ontario
By **Gervais Perron**

Introduction

Based on the results of the 1998 acquisition campaign at Norman West, it was decided amongst the Consortium's participants to go back to Falconbridge's property in Sudbury to answer important questions regarding survey geometry, tool performances and the radius of investigation of the DSI technology. The '98 data showed poor signal quality on both horizontal component data. After analysis of the data, it was concluded that this was due to insufficient horizontal offset between the sources and receivers and week receiver coupling with the borehole walls.
Despite those problems, last year's data did identify diffractions associated the ore zone intersecting boreholes N-33 and N-26 and mapped the SIC (Sublayer Norite and Late Granite Breccia) units more that 500 m away from the recording boreholes. It also imaged an horizontal fault systems within the Norman West embayment and distant diffractors outside of the known limits of mineralization. This proved the success of the method to identify ore bodies and key stratigraphic units in the immediate vicinity (within 500 m) of known mineralization.
For the 1999 campaign, a new set of goals was put forward. The question of radius of investigation versus confidence level and acquisition cost was critical information needed to assess the cost benefits and viability of the proposed exploration technology. Thus, a new geometry design, including recording boreholes located as far as 1.5 km away from the Norman West deposit and source offsets beyond one kilometer, was selected for the 1999 Norman West DSI survey.

Survey Design

The 1999 survey design was largely based on last year's geometry and included 5 source points in a cross pattern, the middle point located between both recording boreholes. Boreholes N-40 and N-43 were chosen as recording holes because of their relative distance from the known Norman West embayment structure. While last year's recording holes (N-26 and N-33) were intersecting the ore zone, N-43 and N-40 are respectively 700 m and 1.5 km west of it. This recording hole selection was made to answer Falconbridge's question about the detectibility range of the method. Can the DSI technology locate the Norman West embayment structure and mineralization from 500 and 1000 m?
The other main difference from the 1998 survey design is the use of larger source-to-receiver offset. Besides the Central shot point used for velocity estimations and profiling purposes, all 4 remaining shot points had offsets from the borehole collar ranging from 400 m (West) up to 2500 m (North) (see Fig.15.1. With these kinds of offsets we can assure that a sufficient amount of energy will be recorded on the horizontal geophones, thus, making sure that the rotation of the horizontal components will be accurate.
Note that the West, Central and East shot points and both recording boreholes are

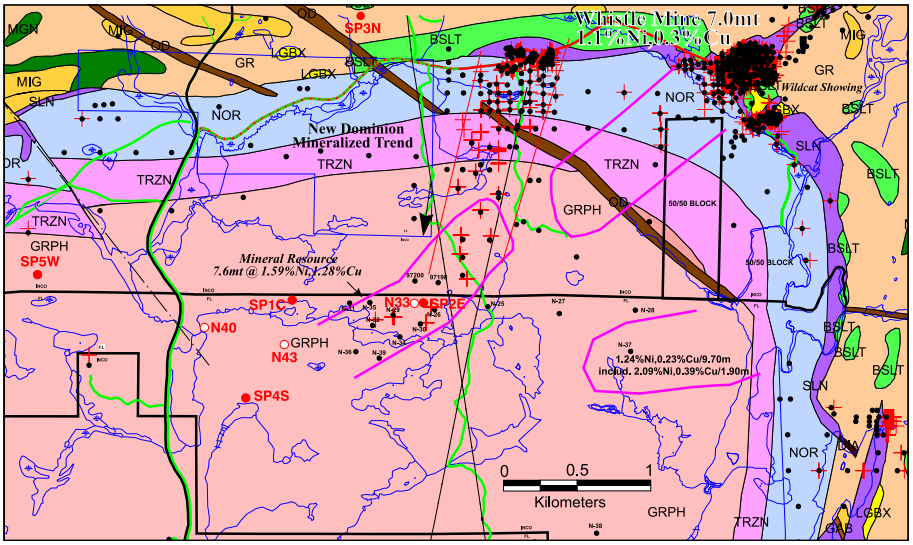

Figure 15.1: Norman West regional geology showing the SIC units, mineral occurences and drillholes. The NW99 survey geometry is indicated in red and includes 5 shot points, 2 recording boreholes (N-40 and N-43) and the N-33 the borehole in which geophysical data were collected

aligned along an east-west trend. The idea behind having this line was to test the use of a tomographic approach to characterize the velocity structure of the SIC units at the Norman West property and hopefully identify a velocity variation associated with the embayment structure.

Surface Geophone

Another important feature that was added for the 1999 survey are surface geophones (2) grouped on the same recording channel and located near the recording borehole collar. The purpose of the surface geophones is to estimate the relative clock drifts between each blasting boxes and the seismograph's triggering system. These surface geophones remain at the same location for the duration of the survey, thus, any delay between the first break arrivals of the first shot of the survey and any subsequent shot can only be attributed to clock drifts since the source and receiver locations are kept constant (Fig.15.2). This method can also be useful to reveal errors in the observer notes, since every shot point has a characteristic travel time associated to it, making it easy to identify from which shot point a specific record belongs to.

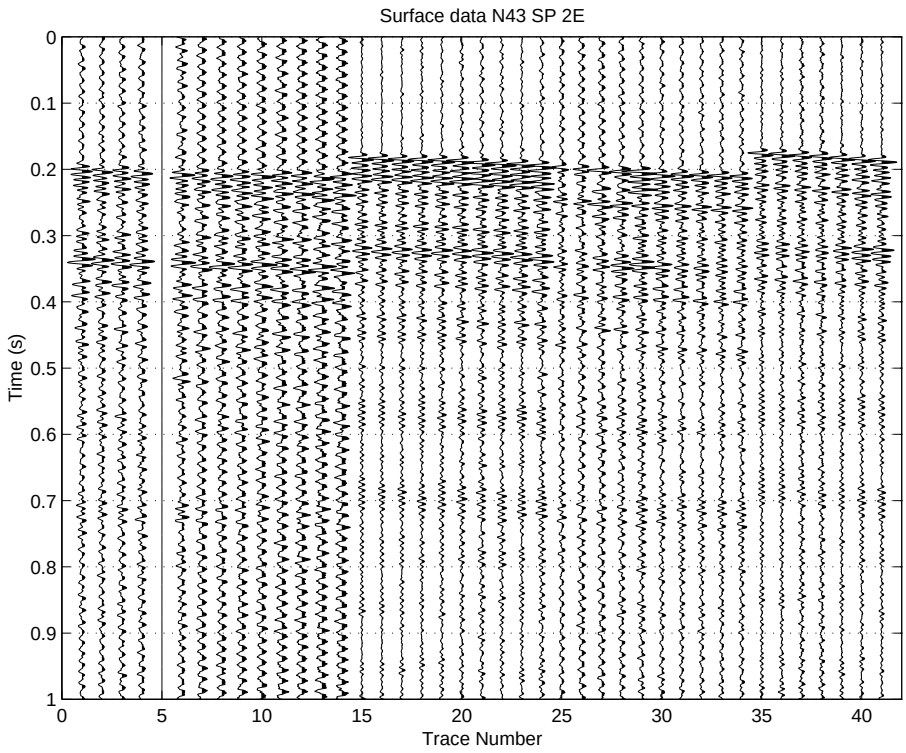

Figure 15.2: Example of a surface geophone data from the N-43 survey. All traces are coming from the shot point 2E. Misalignment of the first break arrivals are dur to relative drifts between shooting boxes.

Recording Parameters

Five VSP's per recording hole were collected. The recording depths ranged from 350 m to the end-of-hole (1419 m and 1705 m for N-40 and N-43 respectively). The recording interval was 5 m for the entire survey. Records were 3 seconds long on all 25 channels (13 when using the 4-level tool) including the surface geophones. The time sampling interval was 1/4 of a millisecond providing non-aliased data up to 4000 Hz. No frequency filters were used at the recording stage. The recording toggled between 24 and 48 dB depending on the shot point and depth of the receivers. Observer notes were taken for every shot, including, Field File ID (FFID), shot point ID, blasting box number, recording depth and comments. An OYO DAS-1 from rented OYO Geospace in Calgary was used as the recording seismograph.

Sources & Receivers

The data were collected using an eight level 3-component geophone chain from Vibrometric Oy (Finland). Each receiver level was equipped with a stabilization ring (see tool update report) and a short (40 mm) clamping arm for maximum stability and leverage force (Fig.15.3). A bad electrical connection on the third clamping motor dictated the usage of the GSC's own 4-level chain as a backup recording system for the first 280 m of borehole N-43. The chain was repaired on site within hours by Vibrometric technicians and was used for the remaining part of the survey.

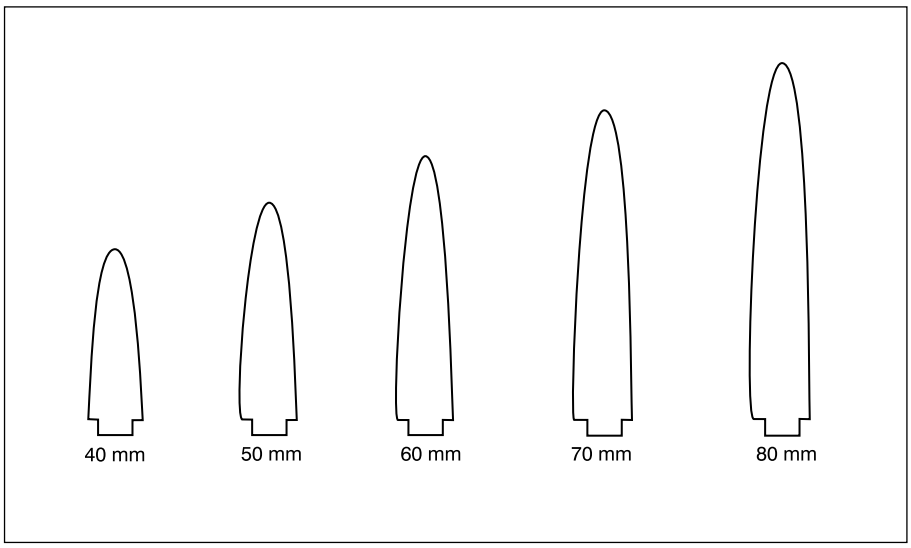

Figure 15.3: Example of the range of clamping arms length available to the Vibrometric geophone chain. This year, the 40 mm arm was used with success. Longer arms are designed to be used in larger boreholes (HQ). Technicians have used the tool without clamping arms in BQ boreholes. The clamping is then provided by the small steel piece on which the clamping arm is usually installed.

As for the 1998 survey, 5 shot points were used this year. At each location, three shot holes were drilled to a depth of 5 m and running water was supplied through a network of pumps and hoses. The collar position of each blasting site was surveyed using differential GPS systems, accurate within 50 cm. Blasts consisted in 227 g boosters of Pentholite and zero-delay seismic caps with a 10 m lead wire. Charges were increased to 454 g (1 pound) for the North and South to compensate for large offset and poor shot hole conditions respectively.

Field Acquisition

It took a crew of 9 people 9 days to complete the entire survey. The crew was composed of 5 shooters, 2 observers, 1 trouble shooter and 1 winch operator. As last year, field support from Falconbridge was mandatory to the success of the survey. Jim Bald and Chris Goulet were on site daily and helped in task like maintaining pumps, driving the skidder, ensuring good radio communication, dummy probing the recording holes, etc. Falconbridge also provided access to the South shot point by opening a new skidder road.
Access to the recording holes was made easier for two different reasons. First, N-40 was located about 50 m east of highway 545 running north-south from the town of Capreol. On the other hand, N-43 was located at a remote site on a hill. The winch and trailer were put on a "sloop" used to carry drilling rods to drill site and towed with a skidder just like a giant sled (Fig.15.4). The trailer remained on the "sloop" for the duration of the survey at borehole N-43 and carried back to the highway at the end of the entire survey.

Figure 15.4: Image showing how the winch and trailer was transported from N-40 to N-43. A sloop designed for moving drilling rods was used to carry the DSI equipment.

Each shooter had his/her own blasting box. All 5 shooting box were synchronized every day with a sixth box used as a triggering system for the seismograph. Due to the increased offset between the shooting sites and the recording borehole, it was impossible to physically link each shooting box to the seismograph. As mentioned above, relative drifts between boxes (usually less that 20 ms/day) were corrected using permanent surface geophones.

In order to get statistical estimates of the random position of the horizontal components at each recording level, all 5 shots were fired before the receiver chain was moved towards the bottom of the hole. The data are then looked over level by level (all 5 shots for 1 depth of recording) and a direction of the H1 component is picked by the processor based on the statistical results from the rotation analysis. This procedure is well explained in the Processing Report of the Norman West '99 data by Gilles Bellefleur.

Data Quality

The data quality varied from shot point to shot point. The better results were observed at shot points Central, East and North. These data were of better signal-to-noise ratios and higher frequency content. Consequently, first break arrivals and even reflection could be observed on the raw data (Fig.15.5). But other source locations (South and West) suffered from source generated noise, unusually strong shear wave contamination and predominant lower frequency content (Fig.15.6). We observed that source points located on topographic highs generated more shear waves and lower frequency data probably due to waves reflecting from the hill sides and poor rock competency (higher percentage of fractures).

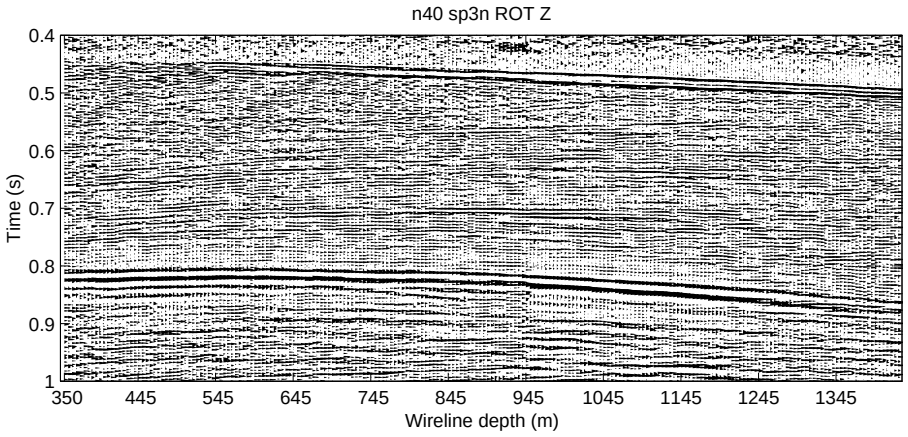

Figure 15.5: Raw rotated data from borehole N-40 shot point 3N. Note the reflected arrival below the P-wave first break arrivals. A small window agc was used for display purposes only.

Sources of noise were of many types. A high tension electrical line runs through the Norman West property and some 60 Hz noise were present on the raw data, but not strong enough to over print the first break arrivals. Thus, a quality check on the data in the field (in real time) was still possible. Capreol is the switching terminal for trains coming from western Canada. From this town trains are either going towards Toronto

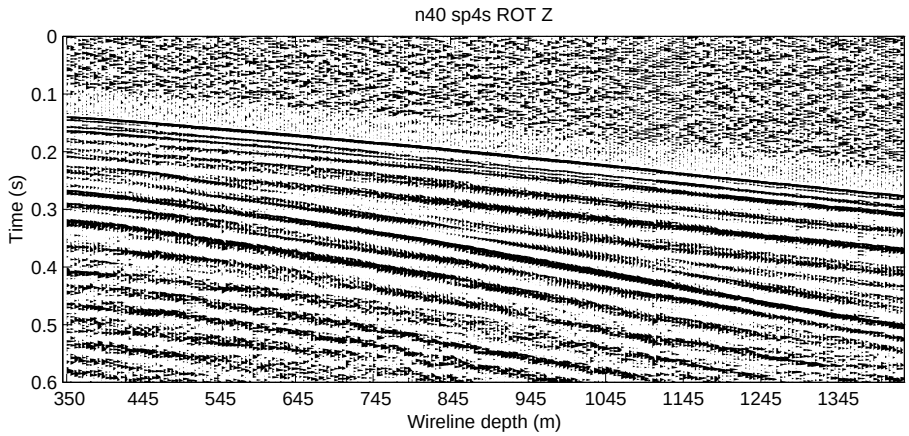

Figure 15.6: Raw rotated data from borehole N-40 shot point 4S. Note the strong P and S wave signature. The ringing is due to the fact tha the shot point was located at the top of a steep hill. The blasting energy was trapped in the topographic feature reflecting of its sides.

or Montreal. On rail system was running west and parallel to highway 545 generating low frequency noise on the VSP records. It was then decided to delay acquisition in the presence of trains. Other sources of noise were caused by the borehole itself. Major fault systems intersecting the boreholes were associated with inflow of water causing tube waves to travel up and down the borehole path reflecting from the water/air interface and the bottom of the hole (Fig.15.7). Another case of tube wave was encountered as the receiver chain approached the bottom of the hole. Moving the tool down the borehole must have a small amplitude wave trapped between the bottom of the hole and the top receiver of the receiver chain. Since the bottom of the hole was near the tool the tube wave did not get attenuated before being reflected (Fig.15.8). This was observed only in the last 100 m of each hole. It was then decided to wait 2 minutes after each move to let the tube wave dissipate. All these sources of noise did not affect the data quality enough to alter the interpretation as most of them were filtered out during the different processing stages.

Conclusion & Recommendations

Many adjustments were made during the NW '99 survey to improve data quality, sub-surface coverage and cost benefits analysis. This resulted in longer shot-receiver offsets (in the order of more than half the receiver depth), different clamping arm length and stabilizing rings for better receiver coupling and stationary surface geophones for clock drifts corrections. But it is still important to keep on shot point close to the recording borehole collar. This enables to compute accurate interval

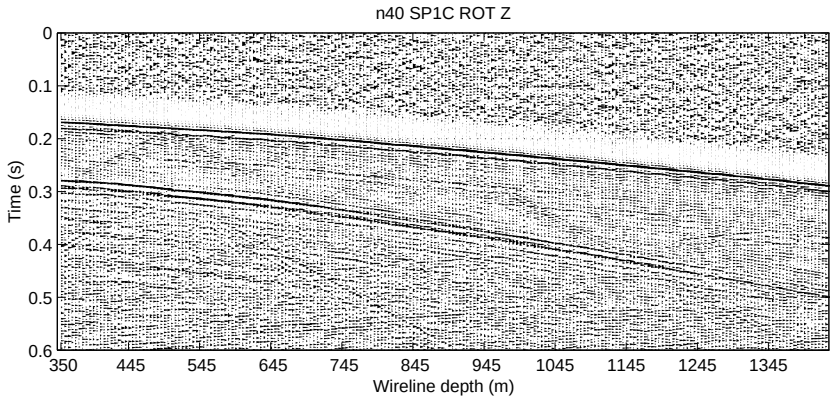

Figure 15.7: Raw rotated data from borehole N-40 shot point 1C. Triangular features are tube waves originating from major gouge fault systems intersecting borehole N-40.

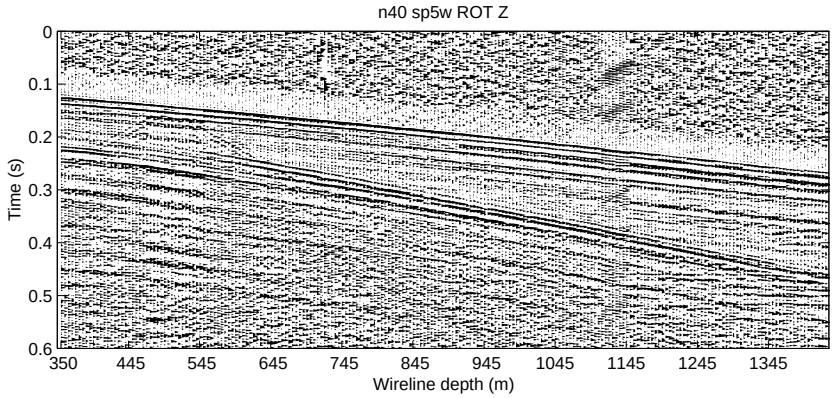

Figure 15.8: Raw rotated data from borehole N-40 shot point 5W. Features isolated on 8 traces and dipping to the left with a P-wave water velocity is corresponding to tube waves generated at the bottom of the recording borehole.

velocity profiles, a reliable average P and S-wave velocity for imaging purpose. It also provide a better distribution of mid-points, closer to the borehole, enhancing the image resolution resulting from the CDP Transform processing.
Selecting shot points in low topographic areas (usually close to lakes) is also important to insure the best data quality possible. It is better to make a compromise on azimuth and offset to select a site that can give you better shot coupling, higher frequency content and less source generated shear wave noise.
Over all, many small adjustments in DSI field acquisition and survey design protocols contributed to the best data quality collected so far by the Consortium's scientists.

Chapter 16

Processing of Norman West '99 Data

By Gilles Bellefleur and Gervais Perron

Summary

This report summarizes the processing performed on the 10 Norman West VSP datasets acquired in Falconbridge's borehole N-40 and N-43 in November 1999. The processing sequence is relatively similar to the one used last year. However, due to the 1999 survey geometry and the availability of new processing modules, some processing steps provided improved results. They are described below. 1) First break discontinuities caused by synchronization of the shooting boxes were observed on the raw data. The surface phone placed close to the boreholes provided the information required to estimate the timing clock delays and aligned the first breaks. 2) Clear first breaks observed on all components recorded from all shot points were used to establish the orientation of the tool in the borehole at every depth level. This information was then used for rotating the data to align the radial component in the shot point direction. The larger offsets used during acquisition provided the highest horizontal/vertical components amplitude ratio and consequently, the most reliable rotation angle. 3) The down-going P and S-waves recorded at each triaxial geophone of the 8-level tool have different response and ringing characteristics. Standard median filtering could not remove properly the down-going energy because traces with different P and S-waves characteristics are intertwined when the data is sorted into wireline depth. Better results were obtained by applying a median filter to data sorted according to original channel number (step 1) and to wireline depth (step 2). Using this processing sequence, the relative amplitude between the two horizontal component is preserved and thus meaningfull polarization analysis can be performed during data interpretation.

Introduction

This report summarizes the processing performed on the VSP datasets acquired in boreholes N-40 and N-43. Each borehole had 5 shot sites, producing 10 different datasets. Data acquisition in borehole N-40 was performed with a 8-level tool from Vibrometric. In borehole N-43, the DSI 4-level tool and the Vibrometric tool were used. The processing was done with DSISoft on a PC and a SPARC platform. A summary of the processing flow is listed in table 16.1. A listing of the scripts and data files generated during data processing can be found in appendix. Most of the examples presented in this report are from data recorded in borehole N-43.

Geometry

The first step consisted in converting the SEG2 data to the DSI format. The data was then sorted into 5 different datasets according to shot position. The geometry necessary for future processing steps was assigned to each of the datasets headers. A

datum of 375 m above sea level was chosen and introduced into the trace headers. The same datum was used for the processing of the 1998 Norman West datasets (Mah, 1999).

Shooting box drift static correction

The arrival of the first break energy is discontinuous on the raw data (figure 16.1). The discontinuities are caused by drift in the timing clock of the shooting boxes. Clocks were synchronize at the beginning and the end of each recording day. However, the time difference at the end of one day is not sufficient to correct the data since the drifts are not necessarily linear. A surface geophone placed in the vicinity of the borehole recorded signal from the various shot points. These surface traces (figure 16.2) were used to correct the drifts. The ray from one shot site to the surface geophone followed the same path during the entire survey. The first break arrival

Geometry	
Sort	Wireline Depth
Timing clock drift corrections	
Monofrequency electrical noise removal	Adaptive filter (60, 180, 300 Hz)
Rotation to maximize energy in H1	Based on energy from 6 ms before first breaks to 8 ms after first breaks
Predictive deconvolution of vertical component	Start of window = 50 ms before firstbreaks End of window = 150 ms after firstbreaks Operator lag = 2.75 ms Operator length = 3 ms Prewhitening = 1%
Predictive deconvolution of horizontal components	Start of window = 0 s End of window = 2 s Operator lag = 7.50 ms Operator length = 3 ms Prewhitening = 1%
Resample	Sample rate = 0.5 ms (original 0.1 ms)
Removal of downgoing P-wave	median velocity filter (15 points)
Removal of downgoing S-wave	median velocity filter (19 points)
Removal of tubewave energy	f-k filters (N43) Tube_time (N40)
Removal of other downgoing energy	f-k velocity filter
agc 3 components	
Bandpass filtering	40Hz-70Hz-160Hz-190Hz

Table 16.1: Summary of processing flow for DSI datasets recorded in boreholes N-40 and N-43.

time discontinuities observed on the surface data are therefore produced by timing clock drifts. The drifts were estimated by cross-correlating a reference trace (the first trace except if too noisy) with the surface traces. The calculated time shifts were introduced into trace header 10 and subsequently applied to the data. An example of the drifts obtained for the east shot point is shown in figure 16.3. Figure 16.4 presents the vertical component recorded with the east shot point (N43) after drift corrections were applied. Note that with this approach the relative delay within individual VSPs are accurate but a delay between each VSP dataset can exist.

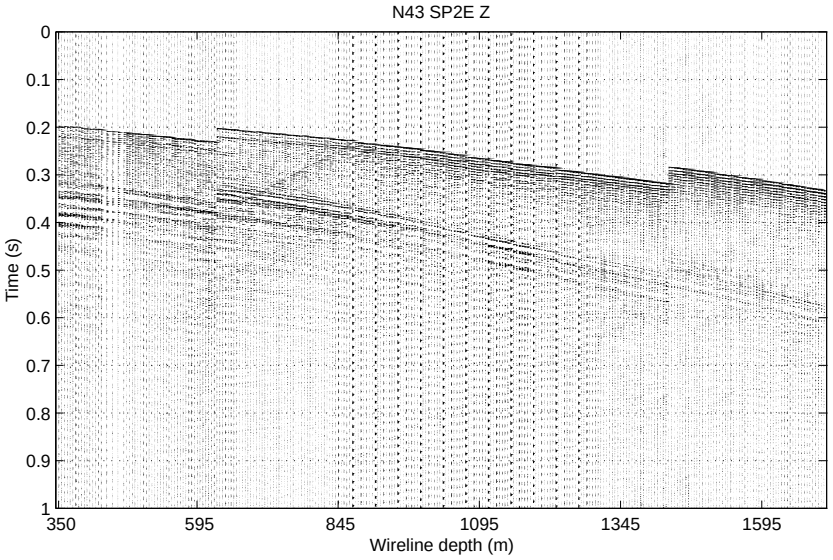

Figure 16.1: Raw data from shot point east, borehole N43. Energy balancing was applied to the traces for display considerations.

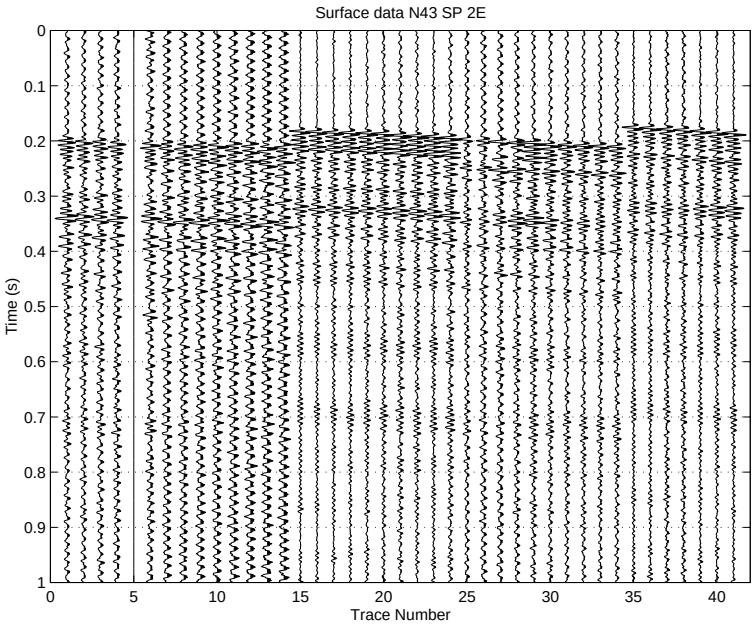

Figure 16.2: Traces recorded with the surface geophone from shot point east. Each trace corresponds to a blast.

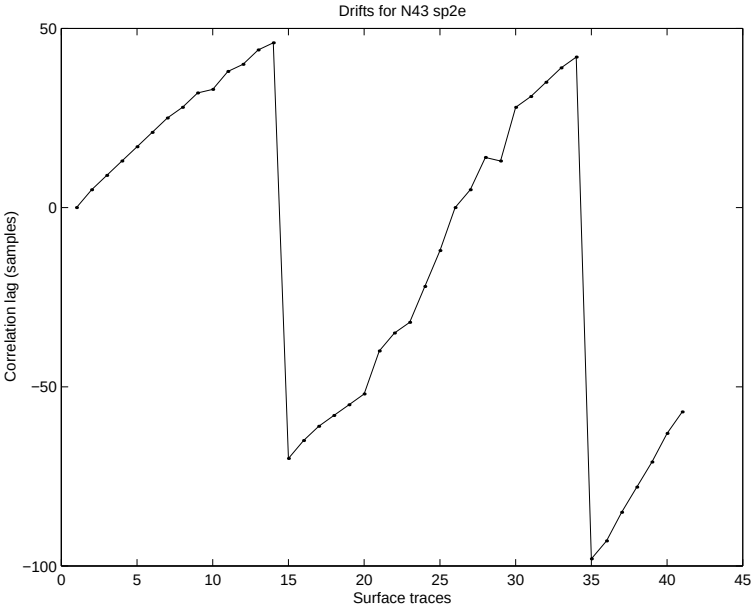

Figure 16.3: Statics corrections obtained by cross-correlating the surface traces. A positive lag corresponds to an increasing time shift.

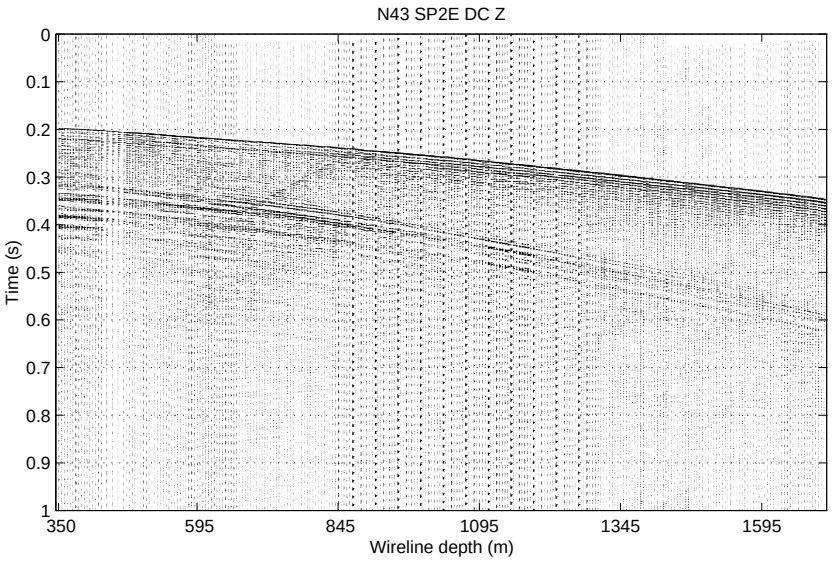

Figure 16.4: VSP data after drift corrections were applied.

Filtering

Moderate-to-low electrical noise contamination were observed on the data. The contamination is significative for shot points with larger offsets, or with lower recorded amplitudes (e.g. lower S/N ratio). Electrical noise at 60, 180 and 300 Hz were removed using an adaptive filtering module (Adam and Langlois, 1995). The data were also filtered with bandpass frequencies between 50 and 250 Hz using low-cut and high-cut frequencies of 25 and 300 Hz with DSISoft Finite Impulse Response (FIR) filtering modules (Mah, 1999).

Rotation Analysis

A rotation analysis was performed simultaneously on data from the 5 VSP datasets in boreholes N40 and N43. This analysis is used to determine the original receiver orientation and the angle of rotation required to maximize the horizontal energy in one component. The energy is calculated in a window of 6 ms before and 8 ms after the first breaks. During acquisition, the receivers were kept at the same position (same orientation) for a specific recording depth, until traces from all shot points were recorded. Thus, a unique receiver orientation at each level must provide a unique rotation angle for all VSP datasets recorded in the same borehole. The analysis was performed on a level-by-level basis. The efficiency of rotation depends on the amount of first break energy on the two horizontal components. Shot points with large offsets (north and west) provided the strongest first break energy on the horizontal components, and for most of the depth level, the most reliable H1 azimuths. However, rotated data from all shot points were analyzed before selecting the azimuth of the H1 component. This procedure ensures that a unique receiver orientation at each level is used during the rotation of the VSP datasets.

Examples of the analysis at wireline depth of 650 m and 1600 m are presented in figure 16.5. The arrows on the compass plot (figure 16.5a ii) indicate the azimuth of the H1 component estimated for each shot point. The locations of the shot points are indicated by the stars on the same figure. The distance from the center of the circle is a function of the shot-receiver distance. At 650 m, the estimated azimuth for H1 is near 290° for the 5 shot points. First breaks before and after rotation are displayed below the compass plot (figure 16.5a iv). Each window corresponds to a specific shot point location. The traces within a window correspond to the H1, H2 and Z components before and after rotation. For an optimum rotation, the fourth trace (H1 after rotation) should have a relatively strong first break, while the fifth trace (H2 after rotation) should have almost no energy. Traces 3 and 6 (vertical component before and after rotation) are identical. At 1600 m, rotated data from 3 shot points converge to the same H1 azimuth (near 170°). However, data from the central and east shot points provided different H1 azimuths (figure 16.5b ii). At

that particular level, the horizontal components for these two shot points display weak and oscillating amplitudes. Rotation of data could not maximize the first break energy on one component. For this reason, the azimuth from these shot points were not considered. At the 1600m level, an azimuth of 170° was selected and used for the rotation of the 5 VSP datasets.

Rotation of horizontal components provided satisfactory results for all shot points. An example from shot point north before and after rotation is shown in figure 16.6. This dataset has the highest horizontal / vertical components amplitude ratio. Data from shot point east before and after rotation are shown in figure 16.7. The horizontal/vertical components amplitude ratio for this dataset were in general lower than the ratio from the north shot point. Figure 16.8 compares results when all VSP datasets and a single VSP dataset (shot point west, N43) are used to estimate H1 azimuth. Results are visually indistinguishable. Subtraction of both rotated data sets exhibits some small differences near the S-wave arrivals.

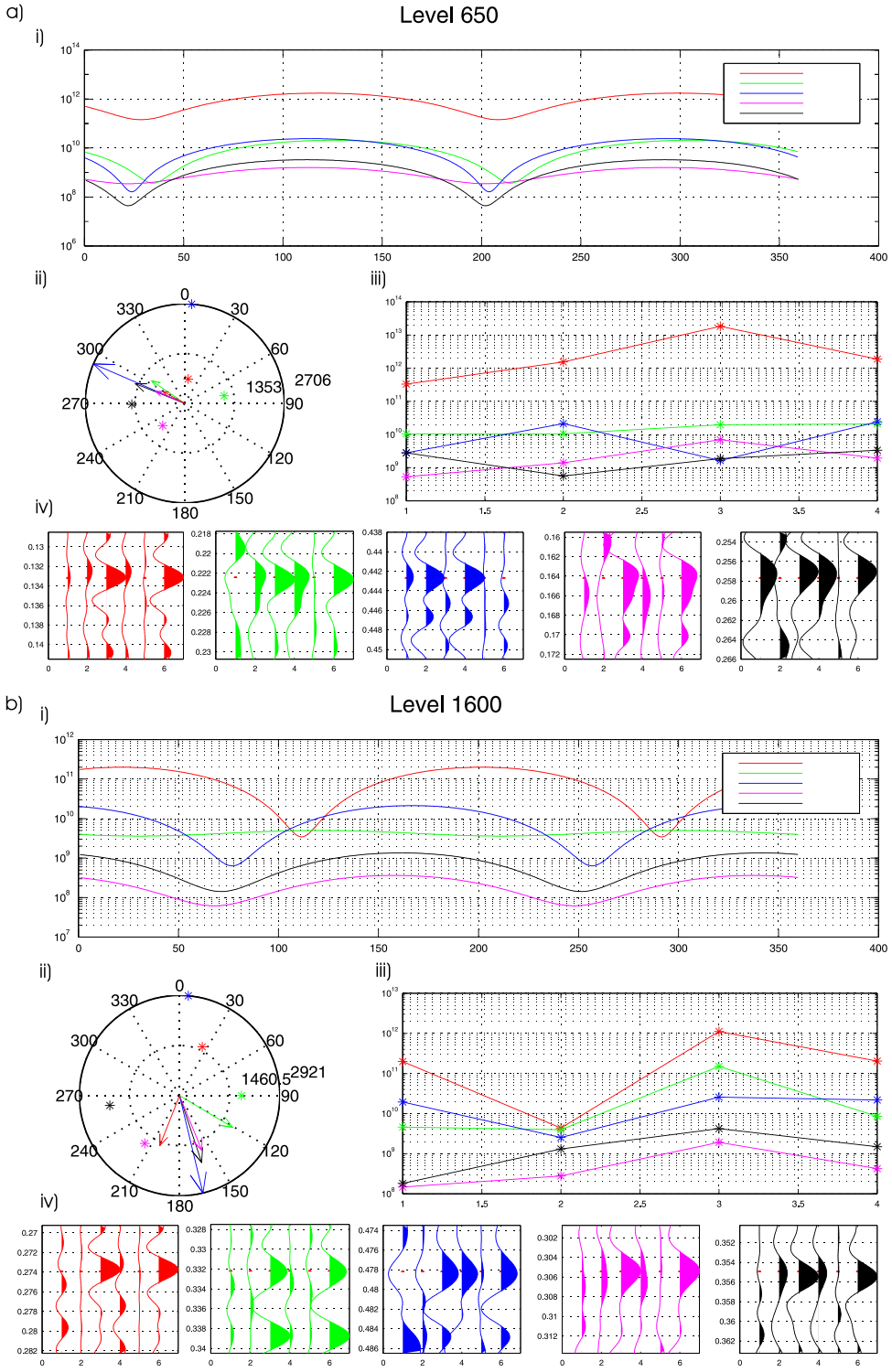

Figure 16.5: Rotation analysis integrating information from the 5 shot points at level 650 m and 1600 m in borehole N43.

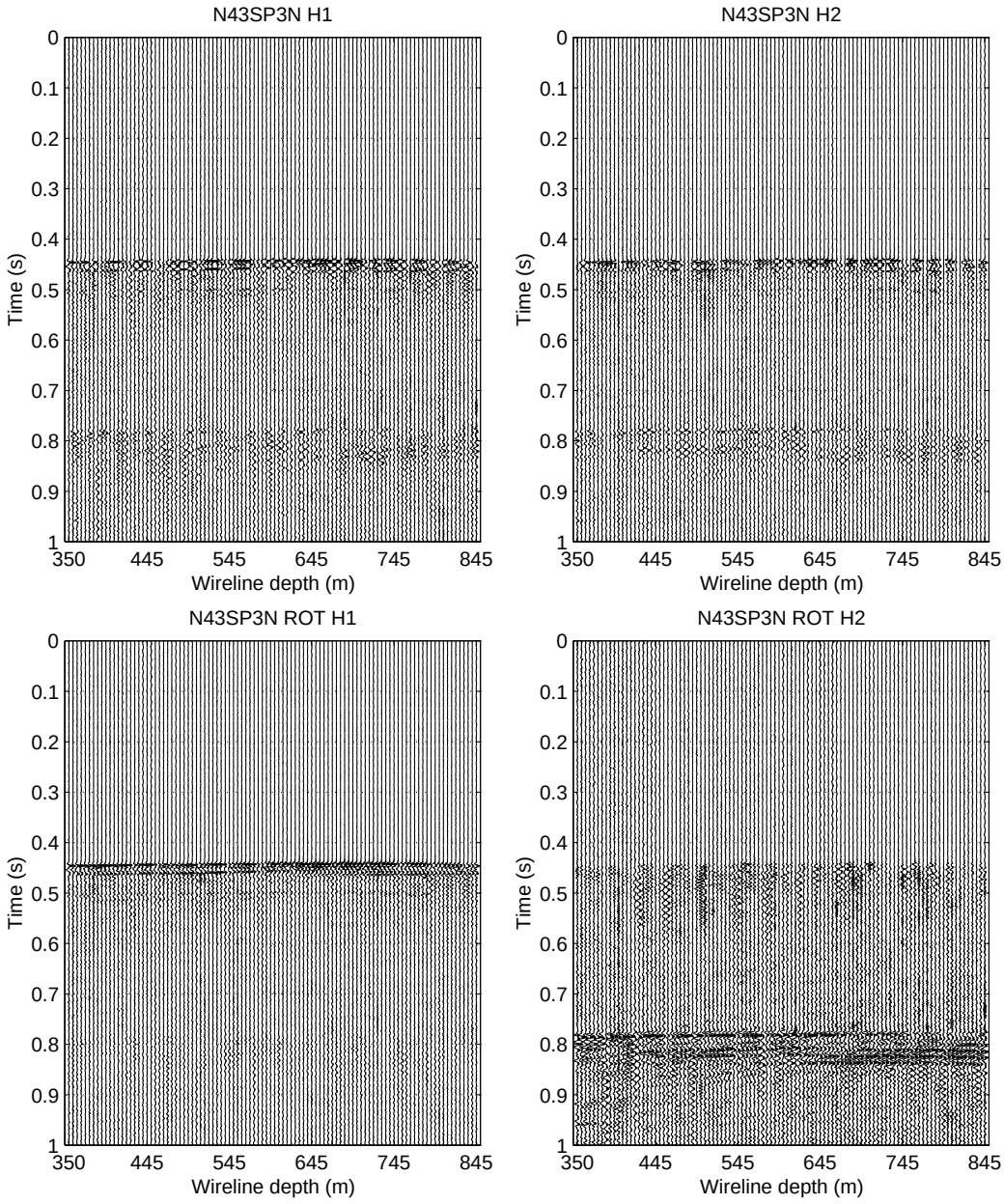

Figure 16.6: H1 and H2 components before and after rotation for shot point north (N43).

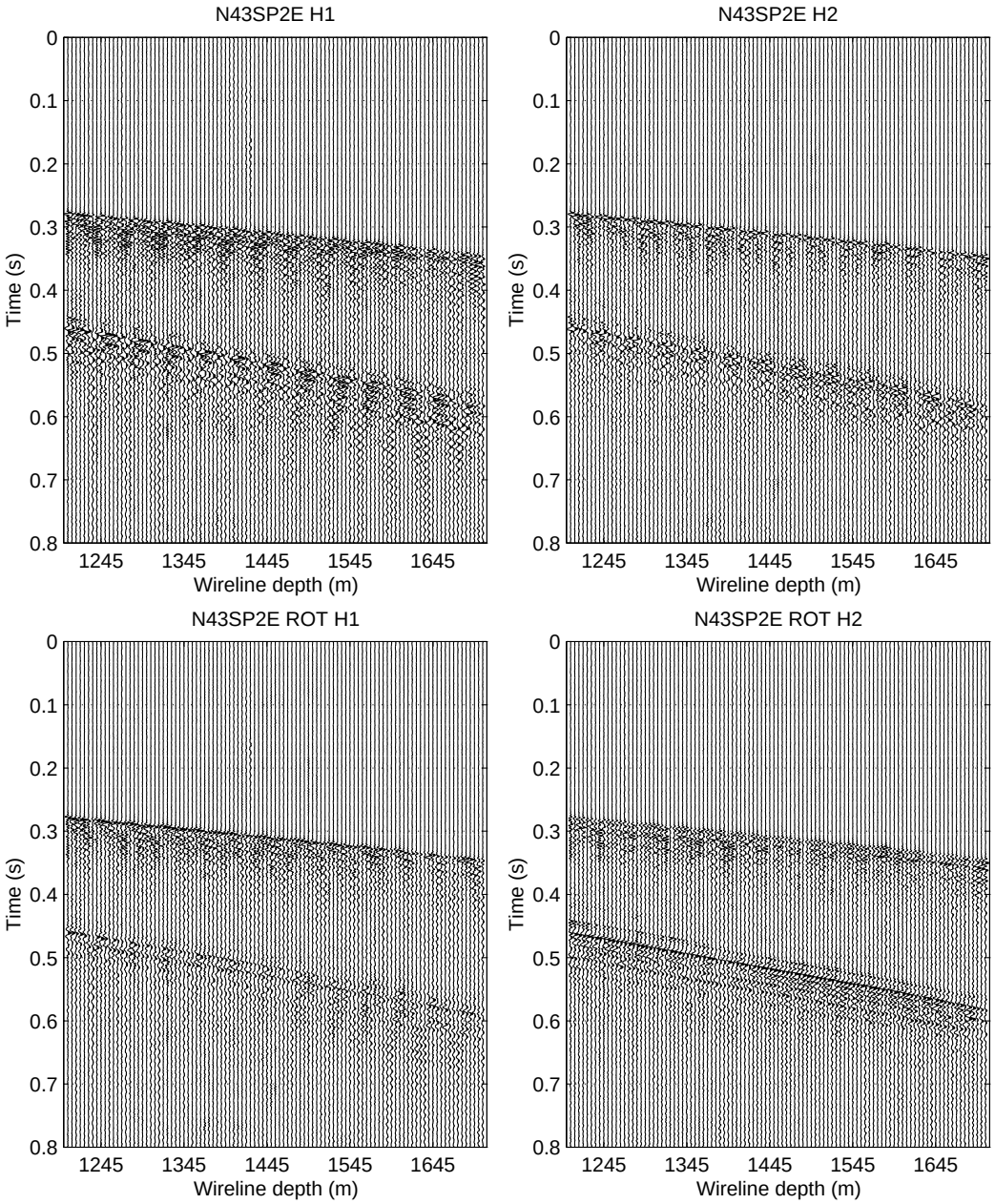

Figure 16.7: H1 and H2 components before and after rotation for shot point east (N43).

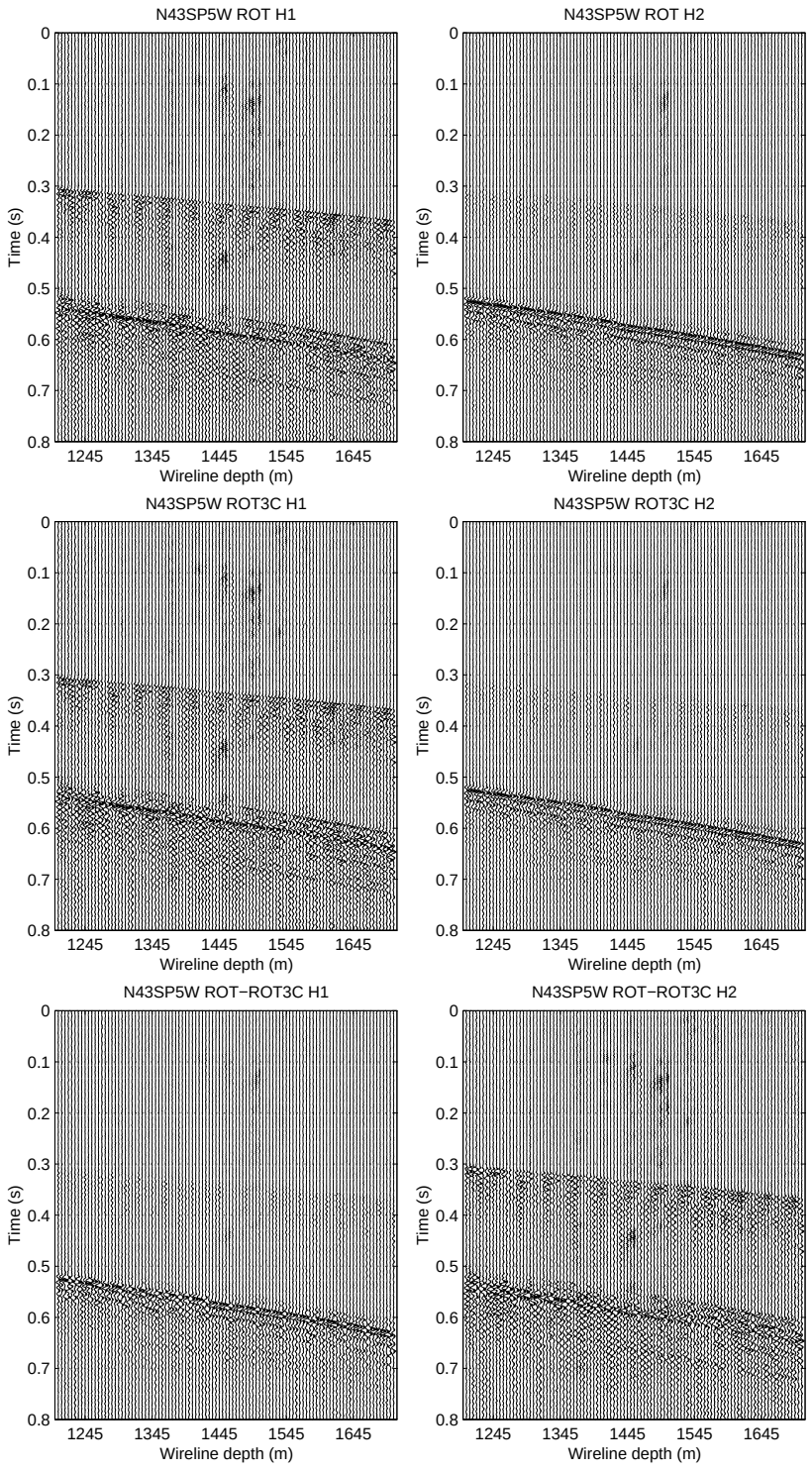

Figure 16.8: Horizontal components from shot point west(N43). Top: H1 and H2 components after rotation based on informations from all shot points. Middle: H1 and H2 components after rotation the SP east VSP data set. Bottom: subtraction of Top and Middle H1 and H2 components. Gain functions are different for each of the subfigures.

Deconvolution and resampling

Seismic events near the first breaks are obscured by short period reverberations (figure 16.9). Predictive deconvolution was applied to the data to remove this reverberation effect. Two different sets of parameters were used, one for the vertical component and the other for the 2 horizontal components. Horizontal and vertical components have different ringing characteristics. The parameters are identical to those used by Mah (1999) and are listed in table 16.1. Other parameters were tested, but did not significantly improved the VSP sections. Figure 16.9 (bottom) presents the vertical component of the central shot point after deconvolution. Short period reverberations were mostly significant for shorter source-receiver offsets. The predictive deconvolution clearly help to improve seismic crosssections before median filters. Predictive deconvolution was followed by resampling of the data to half a millisecond.

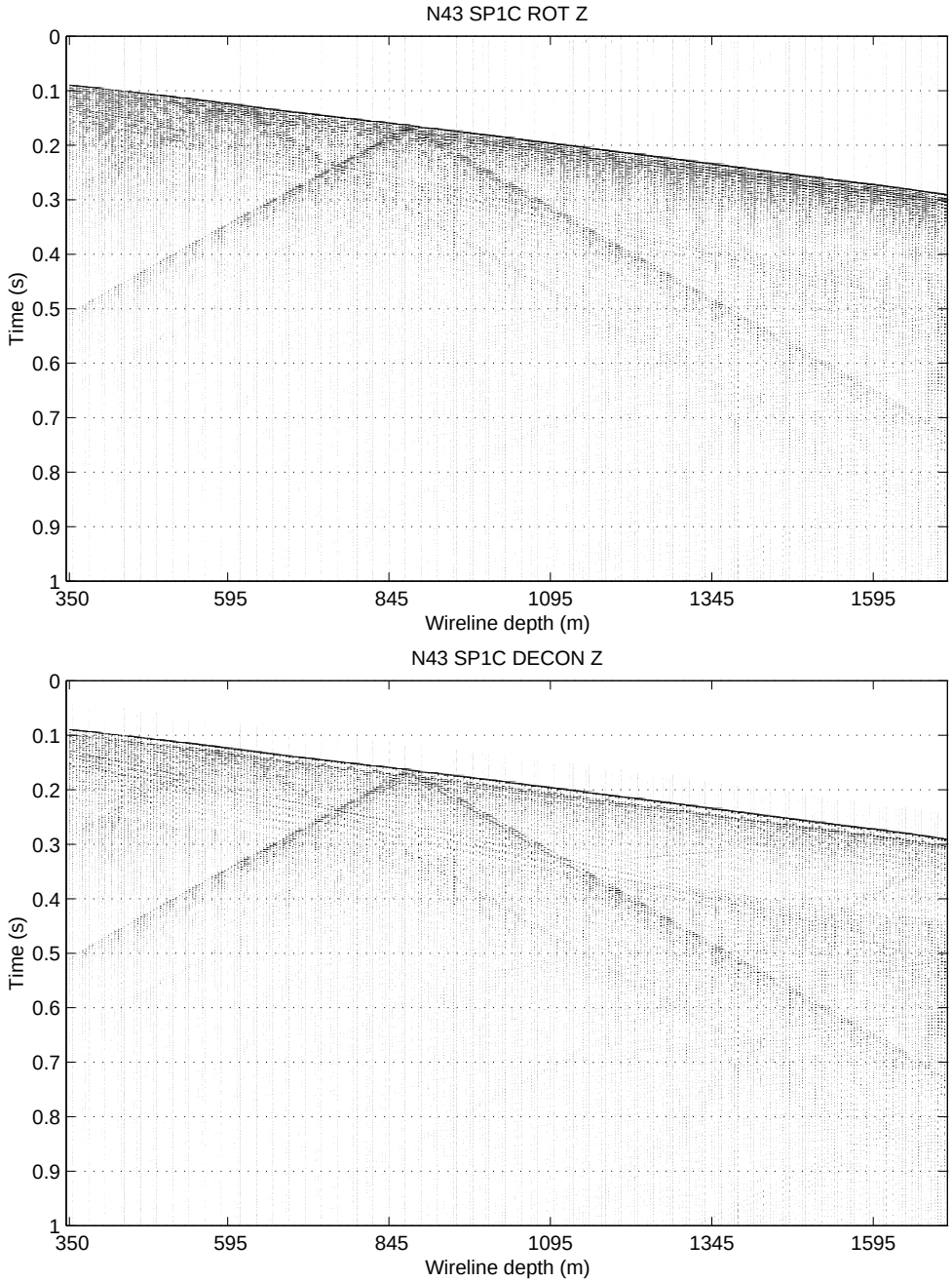

Figure 16.9: Top: Z component from central shot point (N43) before deconvolution. Bottom: Z component from the same shot point after deconvolution.

Median Filtering of downgoing P-waves

First breaks were aligned using manually picked values stored in header 15. A median filter with a filter width of 13 traces was applied to the data. Significant residual amplitudes from the original first breaks are still observed after the application of the filter (figure 16.10). The median filter was not efficient for depth greater than 600 m because the first break waveforms changed from one trace to the other. However, the waveform were relatively similar every 9^{th} trace. This spacing corresponds to traces recorded with the same geophone on the 8-level tool. The 8-level tool was used from 600 m to the end of the borehole (1670 m). Traces in the top part of the borehole were recorded with a 4-level tool. These seem to have a similar first break waveforms for each of the geophone.

Traces recorded with the both the 4-level and 8-level tools were sorted to original channel number. Figure 16.11 shows sorted traces recorded with the first 4 geophones of the 8-level tool. A median filter was applied to the sorted data. The median filter was applied separately for traces recorded with each geophone of the 8-level tool. Traces recorded with the 4-level tool were filtered simultaneously because not enough traces were available to perform a geophone-basis filtering. Traces were sorted back to wireline depth and filtered again with the initial filter width of 13 traces. First breaks and their reverberations (longer period than the one removed with deconvolution) recorded in this borehole are affected by the tool and the local coupling conditions. The two pass of median filter were necessary to properly remove down-going P-wave energy. The VSP data were energy balanced prior to the application of both median filters. The coefficients used during energy balancing were stored and used to remove the gain operator after the application of the filters. This procedure is necessary to preserve the true amplitude of the data to allow meaningfull polarization analysis during interpretation. The transverse horizontal component of the central shot point after median filtering is shown in figure 16.10.

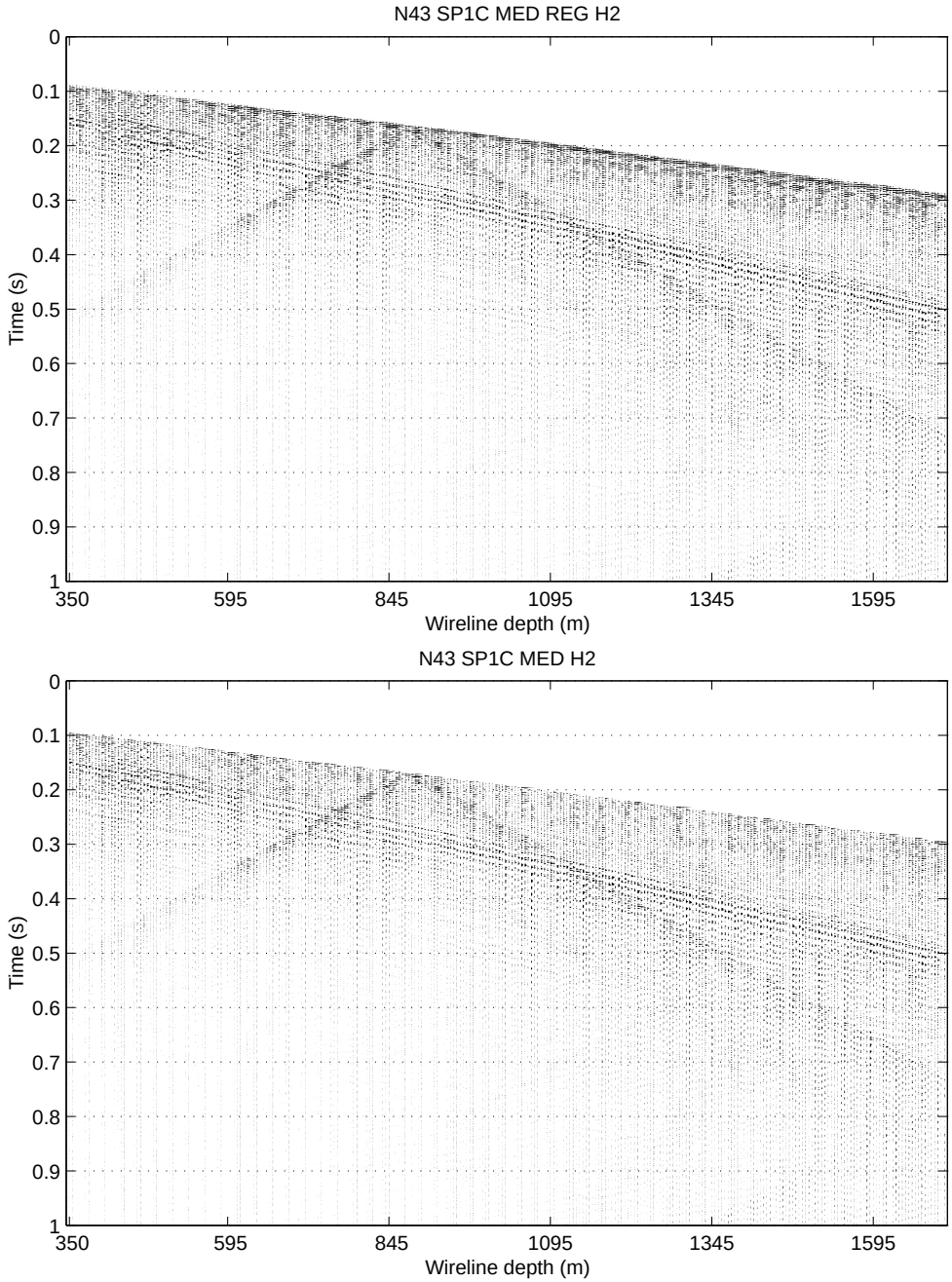

Figure 16.10: Top: Transverse horizontal component from central shot point (N43) after standard median filtering (filter width of 13 traces). Bottom: Transverse horizontal component from central shot point after 2 pass of median filtering (on data sorted by original channel number and data sorted by wireline depth).

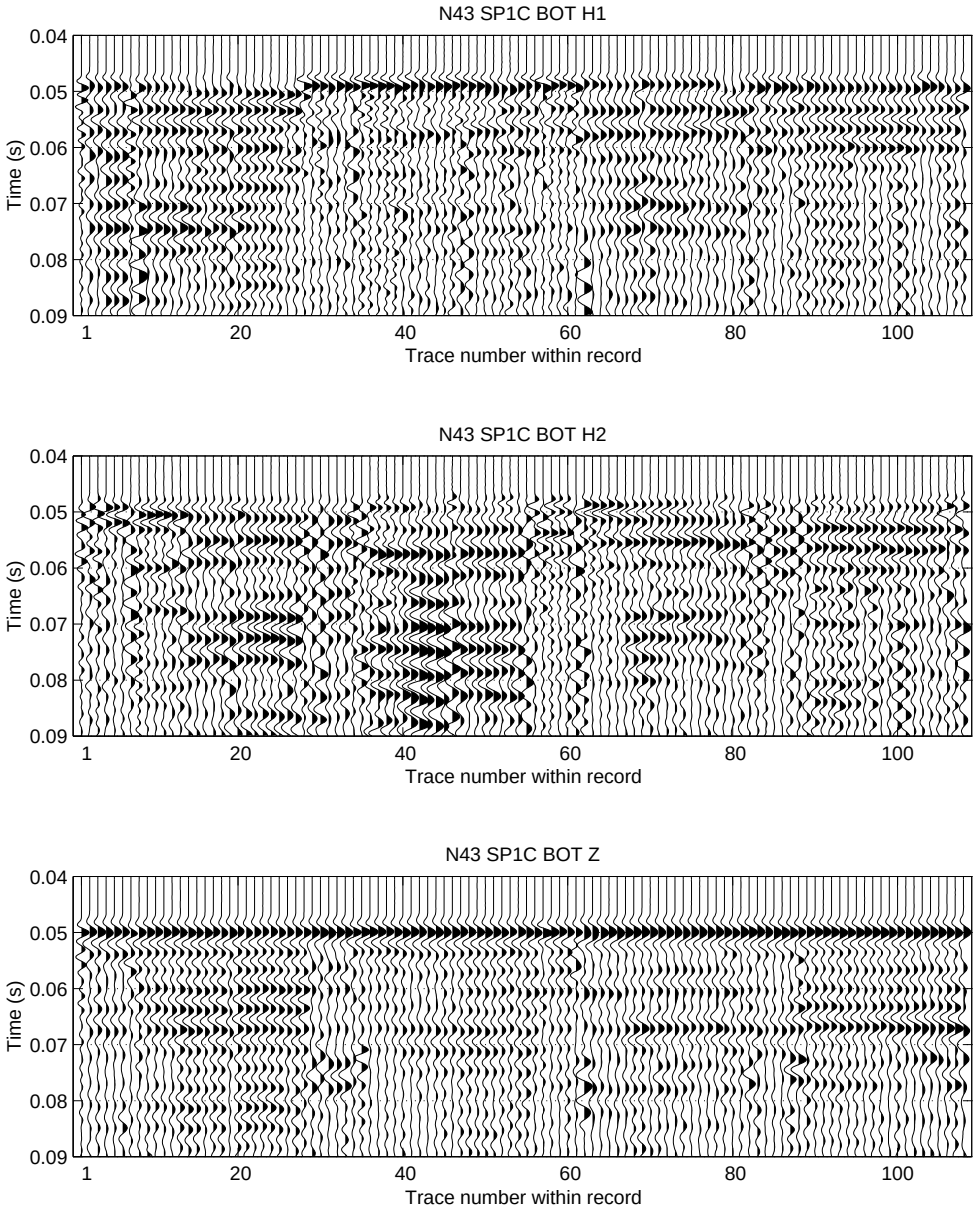

Figure 16.11: Aligned first breaks sorted by original channel number for the 4 geophones of the 8-level tool. Each group of 27 traces were recorded with a specific triaxial geophone. Thus, similarities between the first 27 traces are due to the response of the first geophone on the 8-level tool and are independent of local coupling conditions. Data are from the central shot point, borehole N-43.

Median filtering of down-going S-waves

Similarly to P-waves, the S-waves are affected by the tool and the local coupling conditions (see figure 16.12). Two pass of median filter were also necessary to properly remove the most prominent S-waves. They are particularly significant on data recorded from shot points east, south and west. They obscure other reflections on time windows ranging from 0.1 to 0.2 second. It was decided to apply the two pass of median filter to seismic events located 0.1 s above and below the manually picked S-wave arrivals. Traces recorded with both the 4-level and 8-level tools were sorted to original channel number. A median with a filter width of 11 traces was applied to the sorted data. S-waves with lower amplitudes and lower frequency content were observed outside the main S-wave window (e.g. 0.1 s above and below the manually picked S-wave arrivals). They were removed with a large width median filter (19 traces). This filter was applied to the 2 seconds of data. The vertical component of the southern shot point after median filtering is shown in figure 16.13.

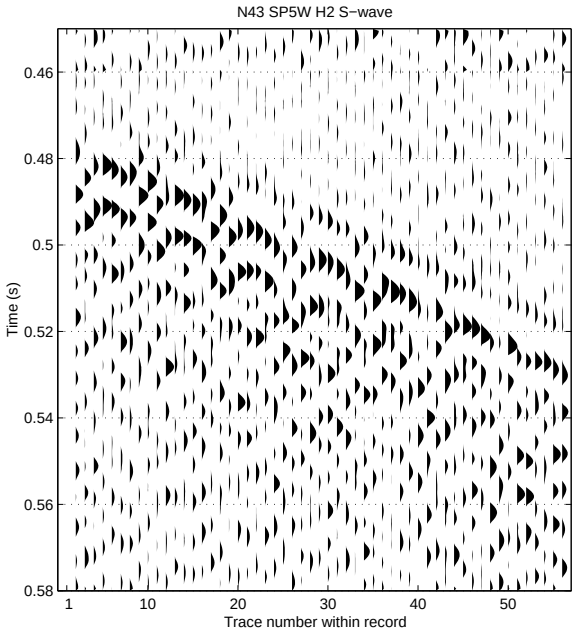

Figure 16.12: S-waves on transverse component from shot point west (N-43) recorded with the 8-level tool. S-wave arrivals are inconsistent and follow a pattern repeated every 9th trace.

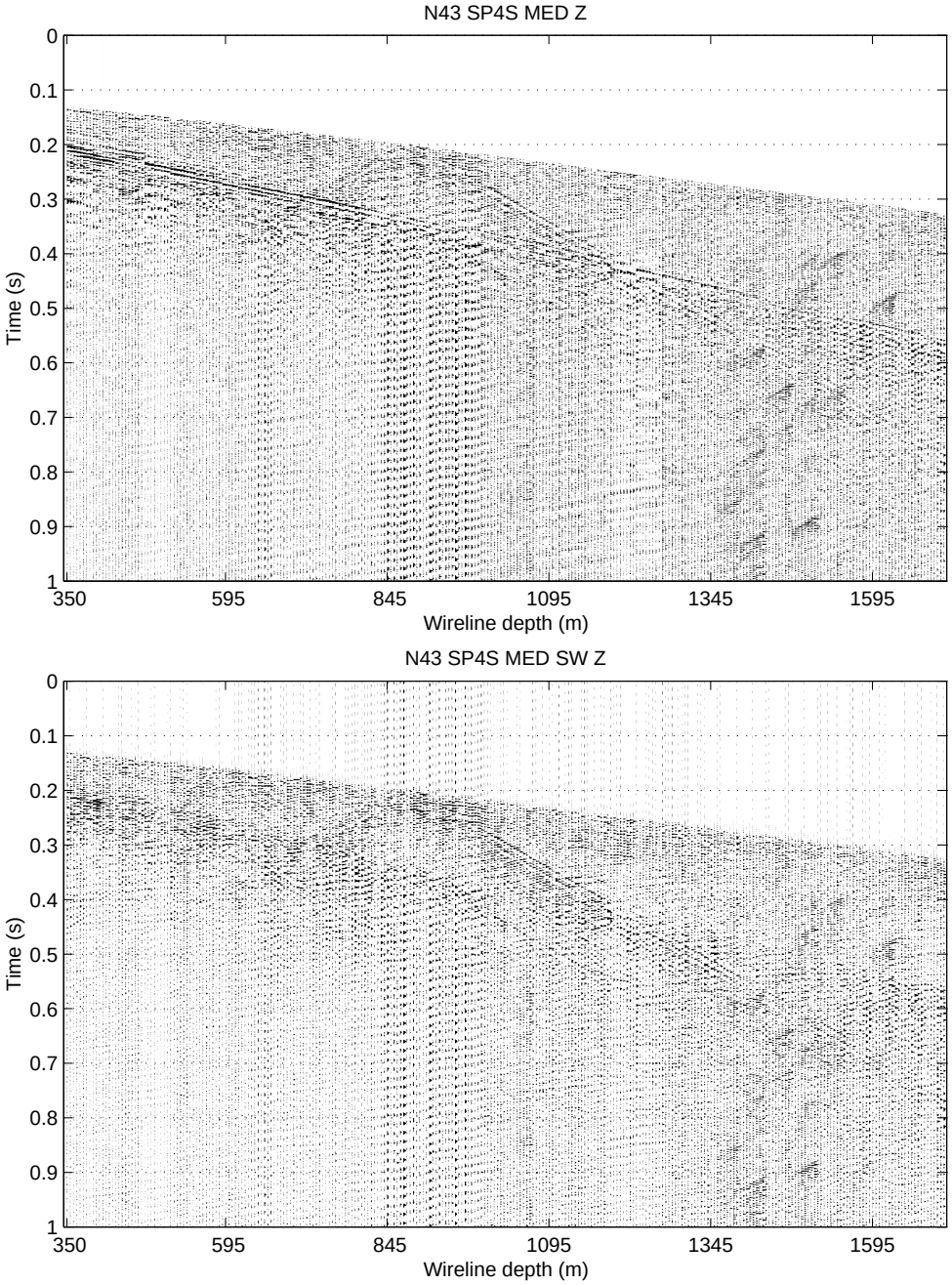

Figure 16.13: Vertical component from shot point south (N43) before (top) and after (bottom) median filtering.

F-k filtering of tube waves

The tube waves are the most striking features after the down-going P and S-wave arrivals are removed. For the VSP datasets recorded in borehole N-43, tube waves were removed with f-k filters. The shape of the filters are similar to those used for the 1998 Norman West data (Mah, 1999). The filters are designed to remove the up-going tube waves with frequencies lower than 225 Hz. The tube_time function (see DSISoft report, this volume) was used to remove tube waves for the datasets acquired in borehole N-40. The residual down-going arrivals were removed with f-k filters for data collected in both boreholes. The vertical component of the central shot point (N-43) after f-k filtering is shown in figure 16.14.

Frequency analysis and bandpass filtering

An agc and a bandpass filter were applied to the fk-filtered data. The higher and lower limits of the bandpass filter were selected from a frequency analysis of the up-going wavefield (figure 16.15). Cutoff frequencies were set to 40 and 190 Hz. The spectrum was totally passed between 70 and 160 Hz.

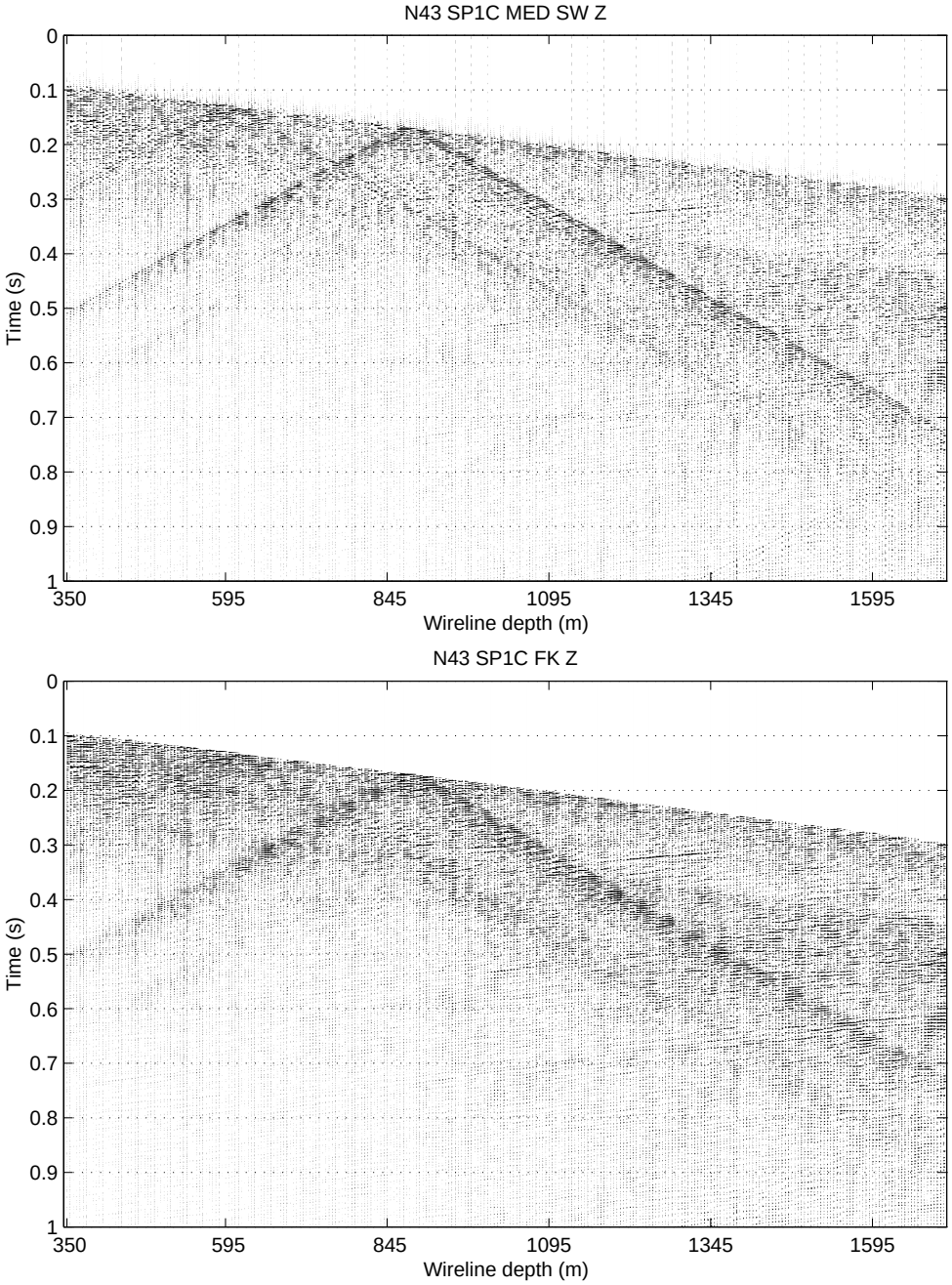

Figure 16.14: Z component from the central shot point (N-43) before (top) and after (bottom) f-k filtering.

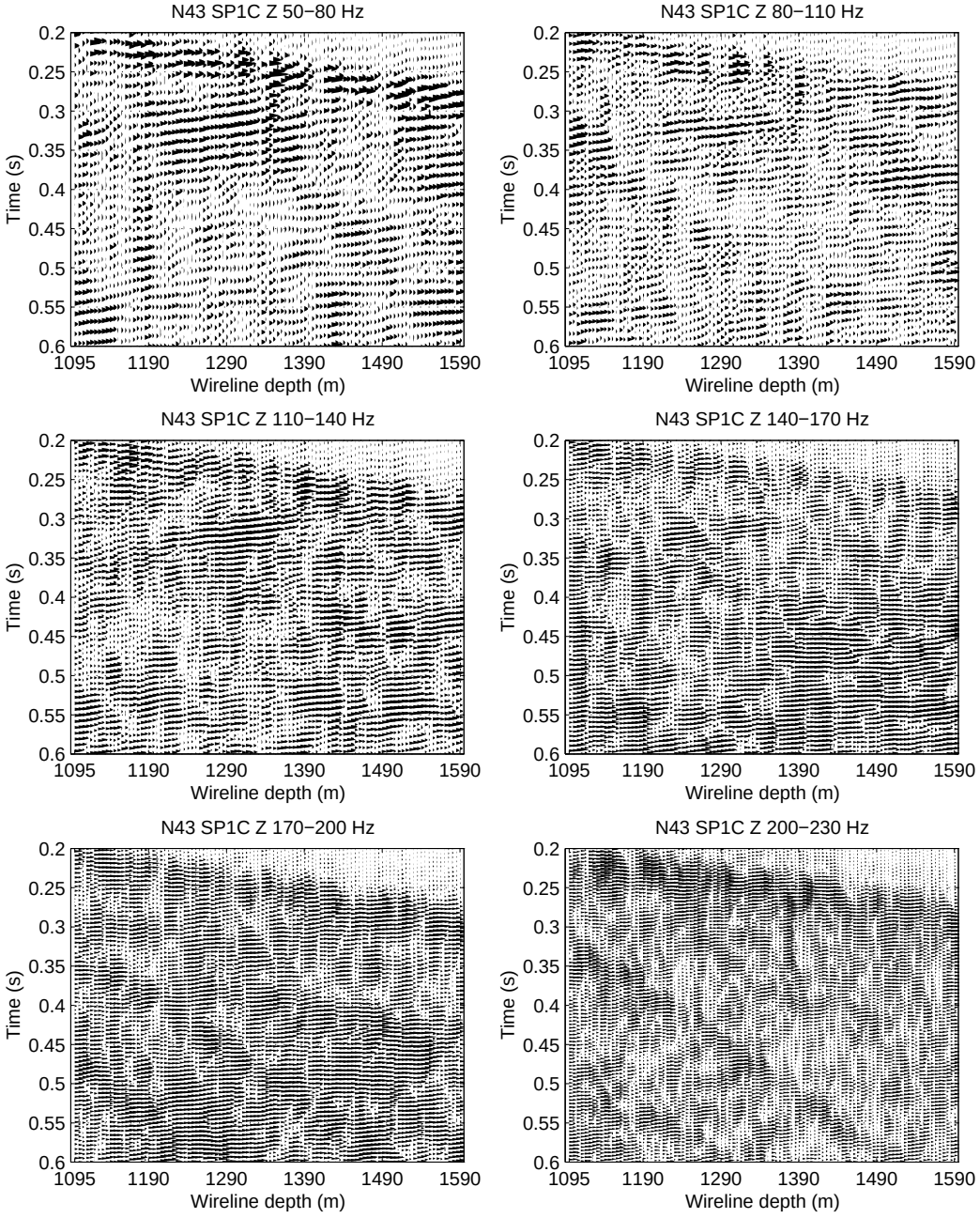

Figure 16.15: Frequency analysis of the vertical component from the central shot point.

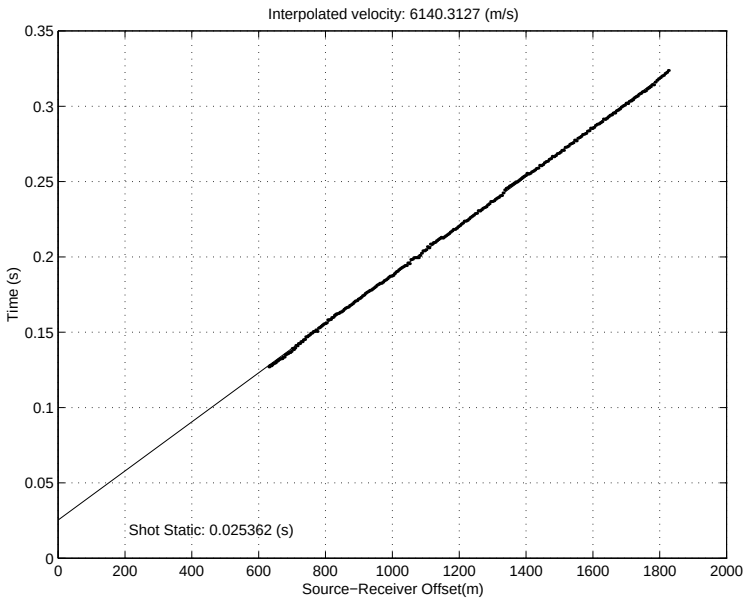

Figure 16.16: Regression of the first arrivals picked on the central shot point data.

Estimation of velocity and zero time offset

The average velocity between a shot point and receivers and the time intercept at zero offset (zero time shift) were estimated by linear regression through the first arrivals (figure 16.16). Data were shifted by the zero time shift to ensure coincidence between modelled and measured first arrivals. The delay at zero offset can be explain by low velocities near the surface or by shooting box delay between different VSP. Results from borehole logging in Norman West hole N-33 show that the granophyre, the first unit intersected in the borehole, has lower velocities than the other lithological units. The granophyre has a thickness of approximately 550 m in the area. The shifted vertical component of the central shot point after agc and bandpass filtering is shown in figure 16.17.

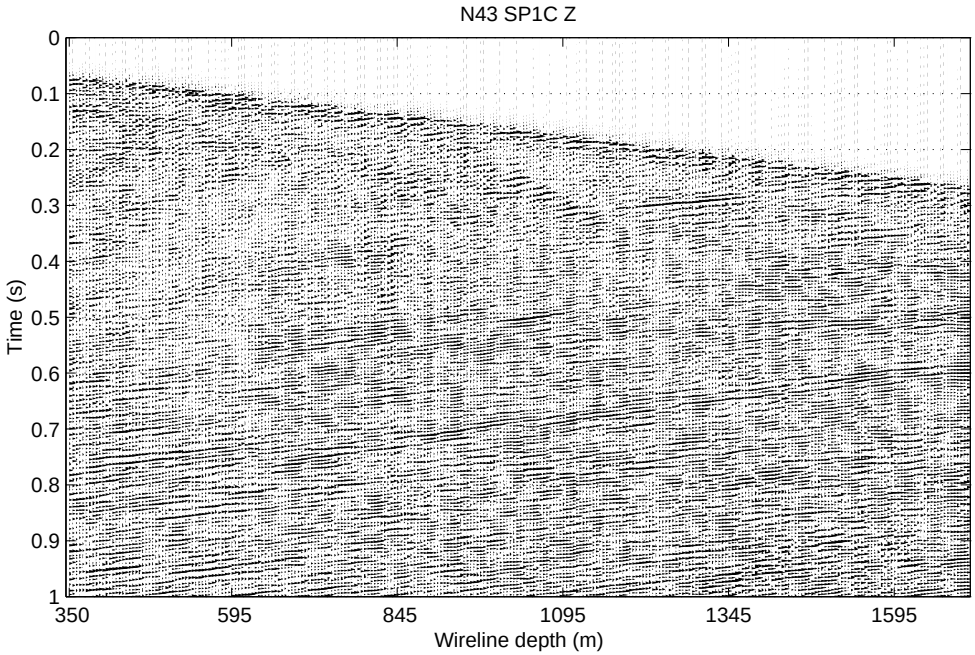

Figure 16.17: Shifted vertical component of central shot point (N-43) after agc and bandpass filtering.

Conclusions

The processing sequence employed is relatively similar to the one used last year. However, due to the 1999 survey geometry and some new processing modules, some processing steps provided improved results. First break discontinuities caused by drifts in the timing clock of the shooting boxes were observed on the raw data. The surface phone placed close to the boreholes provided the information required to correct the timing clock statics and aligned the first breaks. Clear first breaks observed on all components recorded from all shot points were used to establish the orientation of the tool in the borehole at every depth level. This information was then used to rotate the data to align the radial component in the shot point direction. The larger offsets used during acquisition provided the highest horizontal/vertical components amplitude ratio and as a result, the most reliable rotation angle. The down-going P and S-wave recorded at each triaxial geophone of the 8-level tool have different response and ringing characteristics. Standard median filtering could not remove properly the down-going energy because traces with different P and S-waves characteristics are intertwined when the data is sorted into wireline depth. Better results were obtained by applying a median filter to data sorted according to original channel number (step 1) and to wireline depth (step 2). Using this processing sequence, the relative amplitude between the two horizontal component is preserved and thus meaningfull polarization analysis can be performed during data interpretation.

References

Adam, E. and Langlois, P., 1995. Elimination of monofrequency noise from seismic records. Lithoprobe Seismic Processing Facility Newsletter, Vol. 8, No 1, pp. 59-65.

Mah, M., 1999. Finite impulse response filtering report. Downhole Seismic Imaging for Mineral Exploration, pp. 72-86.

Mah, M., 1999. Norman West 98 processing report. Downhole Seismic Imaging for Mineral Exploration, pp. 40-58.

Appendix

```
Processing steps for Norman west borehole N43 (1999)

the ../ directory is the nw99 directory

====================================
Step #1

 =>extract and convert the seg2 VSP and surface data to DSI format
 =>Corrected wireline depths are inserted into header 56

Input files : the file*.dat in the ../rawdata directory

Scripts to extract VSP data are in ../rawdata:
 create_dsi_n43sp1c.m
 create_dsi_n43sp2e.m
 create_dsi_n43sp3n.m
 create_dsi_n43sp4s.m
 create_dsi_n43sp5w.m

 create_dsi_n43_all.m : apply all the create_dsi_n43sp*.m scripts

Scripts to extract surface data are in ../rawdata:
 extr_surf_n43sp1c.m
 extr_surf_n43sp2e.m
 extr_surf_n43sp3n.m
 extr_surf_n43sp4s.m
 extr_surf_n43sp5w.m

extr_surf_n43_all.m : apply all the extr_surf_n43sp*.m scripts

Output VSP data are in ../n43
 n43sp1c.mat
 n43sp2e.mat
 n43sp3n.mat
 n43sp4s.mat
 n43sp5w.mat

Output surface data are in ../surfacedata
 surf_n43sp1c.mat
 surf_n43sp2e.mat
 surf_n43sp3n.mat
 surf_n43sp4s.mat
 surf_n43sp5w.mat

=================================
Step #2 => Apply the geometry into the data files

Inputs ../n43 directory

 n43sp1c.mat
 n43sp2e.mat
 n43sp3n.mat
 n43sp4s.mat
 n43sp5w.mat

Scripts to apply geometry data are in the ../geom directory:

 assign_geom_to_n43sp1c.m
 assign_geom_to_n43sp2e.m
 assign_geom_to_n43sp3n.m
 assign_geom_to_n43sp4s.m
 assign_geom_to_n43sp5w.m

and (for S-R azimuth)

 apply_s2rgeom.m

Two files are also necessary for this step (files are in ../geom)

 collar_n43.txt
 dev_n43.txt

Output : the same files as the input files in ../n43

Script ../geom/assign_all.m : apply all geometry scripts.

=======================================
Step #3 => Calculate and apply shooting box drift statics

Inputs ../n43 directory
```

```
 n43sp1c.mat
 n43sp2e.mat
 n43sp3n.mat
 n43sp4s.mat
 n43sp5w.mat

Scripts in the ../surfacedata directory :

 calc_drifts_n43sp1c.m
 calc_drifts_n43sp2e.m
 calc_drifts_n43sp3n.m
 calc_drifts_n43sp4s.m
 calc_drifts_n43sp5w.m

Outputs are in ../n43 directory :

 n43sp1c_dc.mat
 n43sp2e_dc.mat
 n43sp3n_dc.mat
 n43sp4s_dc.mat
 n43sp5w_dc.mat

script ../surfacedata/calc_drifts_all.m : apply all calc_drifts scripts

====================================
Step # 4

=> Remove 60 Hz 180 Hz 300 Hz and lowpass of the data (250-300 Hz)
=> also apply a high pass (25-50 Hz)

Input files ../n43 :

 n43sp1c_dc.mat
 n43sp2s_dc.mat
 n43sp3n_dc.mat
 n43sp4s_dc.mat
 n43sp5w_dc.mat

Scripts  in the ../process directory :

  harm_n43_sp1c.m
  harm_n43_sp2s.m
  harm_n43_sp3n.m
  harm_n43_sp4s.m
  harm_n43_sp5w.m

Outputs: ../n43/ dir

  n43sp1c_harm.mat
  n43sp2e_harm.mat
  n43sp3n_harm.mat
  n43sp4s_harm.mat
  n43sp5w_harm.mat


The script ../process/harm_all.m apply all the scripts

====================================
Step # 5

=> Pick FB with pick1comp and put FB into header 15

Input and output files : ../n43/n43sp*_harm.mat

Script ../process/put_fb.m
  copy fb from 1 comp to other comp
  FB were also written to mat files in ../n43 :

  fb_sp1c.mat
  fb_sp2s.mat
  fb_sp3n.mat
  fb_sp4e.mat
  fb_sp5w.mat

Script ../process/reput_fb.m
  reput the fb into the header from the fb_sp*.mat files

====================================
Step #6

=> Estimate the azimuth of h1 based on first breaks from all 5 VSPs.
=> Estimation is performed on a level-by-level basis.

Inputs in ../n43 directory:

  n43sp1c_harm.mat
  n43sp2e_harm.mat
```

```
  n43sp3n_harm.mat
  n43sp4s_harm.mat
  n43sp5w_harm.mat

Scripts in the ../qc_dsi directory

  select_h1_azimuth.m : this script loads all data files, create a subset which
  essentially include fb, sort traces according to level of acquisition
  (15 traces => 5 VSPs* 3components per vsp); qc_dsi create the plots used
  to select the azimuth of h1. These values are assigned to header 11 and
  separately saved to h1_azimuth.mat. Azimuth of h1 has to be entered
  manually for each level (272).

  qc_dsi : create the plots with rotation of the 5 vsps fb

  reput_h1_azimuth.m : reput the azimuth of h1 into header 11 of the
                       data files. loads h1_azimuth.mat in ../qc_dsi.

Outputs in the ../n43 directory (same as the inpout files)

  n43sp1c_harm.mat
  n43sp2e_harm.mat
  n43sp3n_harm.mat
  n43sp4s_harm.mat
  n43sp5w_harm.mat

==================================
step # 7

=> Apply the rotation to the data

Inputs in the ../n43 directory

  n43sp1c_harm.mat
  n43sp2e_harm.mat
  n43sp3n_harm.mat
  n43sp4s_harm.mat
  n43sp5w_harm.mat

Script in the ../qc_dsi    directory

  rot_n43sp1c.m
  rot_n43sp2e.m
  rot_n43sp3n.m
  rot_n43sp4s.m
  rot_n43sp5w.m

 Script rot_n43_all.m applies all rotation scripts

Outputs in the ../n43 directory

  n43sp1c_rot.mat
  n43sp2e_rot.mat
  n43sp3n_rot.mat
  n43sp4s_rot.mat
  n43sp5w_rot.mat

  some tests on n43sp5w:
    n43sp5w_rot3c.mat  : rotation using only rot3c
    n43sp5w_rot_minus_rot3c.mat : n43sp5w_rot.mat - n43sp5w_rot3c.mat


==================================
step # 8

=> Apply decon and resample to 0.0005 sec

Inputs in the ../n43 directory

  n43sp1c_rot.mat
  n43sp2e_rot.mat
  n43sp3n_rot.mat
  n43sp4s_rot.mat
  n43sp5w_rot.mat

Script in the ../process    directory

  decon_n43sp1c.m
  decon_n43sp2e.m
  decon_n43sp3n.m
  decon_n43sp4s.m
  decon_n43sp5w.m

 Script decon_n43_all.m applies all decon scripts

Outputs in the ../n43 directory
```

```
  n43sp1c_decon.mat  n43sp1c_resamp.mat
  n43sp2e_decon.mat  n43sp2e_resamp.mat
  n43sp3n_decon.mat  n43sp3n_resamp.mat
  n43sp4s_decon.mat  n43sp4s_resamp.mat
  n43sp5w_decon.mat  n43sp5w_resamp.mat

================================
step # 9

=> Remove FB with median filters

Inputs in the ../n43 directory

  n43sp1c_resamp.mat
  n43sp2e_resamp.mat
  n43sp3n_resamp.mat
  n43sp4s_resamp.mat
  n43sp5w_resamp.mat

Script in the ../process    directory

  median_fb_n43sp1c.m
  median_fb_n43sp2e.m
  median_fb_n43sp3n.m
  median_fb_n43sp4s.m
  median_fb_n43sp5w.m

 Script median_fb_all_n43.m applies all median fb scripts
 script median_fb_n43sp1c_reg.m apply median filter the "regualar" way

Outputs in the ../n43 directory

  n43sp1c_medfb.mat
  n43sp2e_medfb.mat
  n43sp3n_medfb.mat
  n43sp4s_medfb.mat
  n43sp5w_medfb.mat

  n43sp1c_medfb_reg.mat output from median_fb_n43sp1c_reg.m

================================
step # 10

=> Remove Shear waves with median filters

Shear wave arrivals have to be picked and stored in
HW 16 of the input files. The S-Wave picked times
are also saved in the ../n43 directory

  swp_n43sp1c.mat
  swp_n43sp2e.mat
  swp_n43sp3n.mat
  swp_n43sp4s1.mat (H1 and H2)
  swp_n43sp4s3.mat (Z)
  swp_n43sp5w1.mat (H1 and H2)
  swp_n43sp5w3.mat (Z)

The script ../process/reput_swp.m
reput the s-wave picks into the header 16
from these .mat files

Inputs in the ../n43 directory

  n43sp1c_medfb.mat
  n43sp2e_medfb.mat
  n43sp3n_medfb.mat
  n43sp4s_medfb.mat
  n43sp5w_medfb.mat

Script in the ../process    directory

  median_sw_n43sp1c.m
  median_sw_n43sp2e.m
  median_sw_n43sp3n.m
  median_sw_n43sp4s.m
  median_sw_n43sp5w.m

 Script median_sw_all_n43.m applies all median sw scripts

Outputs in the ../n43 directory

  n43sp1c_medsw.mat
  n43sp2e_medsw.mat
  n43sp3n_medsw.mat
  n43sp4s_medsw.mat
  n43sp5w_medsw.mat
```

```
==================================
step # 11

=> Remove the tube waves with FK filters

Inputs in the ../n43 directory

  n43sp1c_medsw.mat
  n43sp2e_medsw.mat
  n43sp3n_medsw.mat
  n43sp4s_medsw.mat
  n43sp5w_medsw.mat

Script in the ../process    directory

  fk_n43sp1c.m
  fk_n43sp2e.m
  fk_n43sp3n.m
  fk_n43sp4s.m
  fk_n43sp5w.m

These scripts use polygon mat files in the ../n43 directory

 For tube waves:
   n43sp1c_twpol.mat
   n43sp2e_twpol.mat
   n43sp3n_twpol.mat
   n43sp4s_twpol.mat
   n43sp5w_twpol.mat

 For residual down-going waves (including tube waves):
   n43sp1c_dgpol.mat
   n43sp2e_dgpol.mat
   n43sp3n_dgpol.mat
   n43sp4s_dgpol.mat
   n43sp5w_dgpol.mat

Outputs in the ../n43 directory

  n43sp1c_fk.mat
  n43sp2e_fk.mat
  n43sp3n_fk.mat
  n43sp4s_fk.mat
  n43sp5w_fk.mat

==================================
step # 12

=> Frequency analysis to determine the optimum freq. window

Inputs in the ../n43 directory

  n43sp1c_fk.mat
  n43sp2e_fk.mat
  n43sp3n_fk.mat
  n43sp4s_fk.mat
  n43sp5w_fk.mat

Script in the ../process    directory

  freqan_n43sp1c.m
  freqan_n43sp2e.m
  freqan_n43sp3n.m
  freqan_n43sp4s.m
  freqan_n43sp5w.m

Outputs are .pcl files

==================================
step # 13

=> agc + bandpass
=> data are also shitfed according to the zero time
=> obtained by regression (with the velocity.m function)

Inputs in the ../n43 directory

  n43sp1c_fk.mat
  n43sp2e_fk.mat
  n43sp3n_fk.mat
  n43sp4s_fk.mat
  n43sp5w_fk.mat

Script in the ../process directory

  post_pro_n43sp1c.m
  post_pro_n43sp2e.m
```

```
  post_pro_n43sp3n.m
  post_pro_n43sp4s.m
  post_pro_n43sp5w.m

Outputs in the ../n43 directory

  n43sp1c_post.mat
  n43sp2e_post.mat
  n43sp3n_post.mat
  n43sp4s_post.mat
  n43sp5w_post.mat

==================================
The following steps were applied
but are not required for processing
==================================
step # 14

Rotate h1 and h2 componenets every 30 degrees
input files are filtered before rotation
(agc, noch and banpass)

Inputs in the ../n43 directory

  n43sp1c_fk.mat
  n43sp2e_fk.mat
  n43sp3n_fk.mat
  n43sp4s_fk.mat
  n43sp5w_fk.mat

Script in the ../process directory

  rot_rx_n43sp1c.m
  rot_rx_n43sp2e.m
  rot_rx_n43sp3n.m
  rot_rx_n43sp4s.m
  rot_rx_n43sp5w.m

Outputs are .pcl files
```

Chapter 17

Interpreting the 1998-99 Norman West Survey
By **Dave Snyder**

Introduction

The DSI consortium's main field project in 1999 was conducted within the Norman West property of Falconbridge on the northeast range of the Sudbury impact structure. Its purpose was to extend the results of the previous year's survey to greater offsets in order to evaluate the ability of multi-VSP surveys to detect sulfide ore bodies at distances greater than the 0-500 m range studied in 1998-99. Receivers were located in holes N-40 and N-43 (Figure 1). Target ore deposits at 1600-2000 m depths were previously identified by drilling and downhole EM methods and successfully imaged by DSI last using receivers at 100-1855 and 100-1915 m depths in holes N26 and N33, respectively. The ten overlapping VSPs acquired in 1998 had a maximum horizontal source-receiver offset of 350 m. The small offsets, combined with high noise levels on the two horizontal components, limited the utility of the data set. In 1999, source-receiver offsets as large as 2500 m were used and horizontal seismometer signal-to-noise ratios were improved to match or exceed those of the vertical components (Figures 2-4).

Geological Setting

The homogeneity and smooth velocity gradients within the granophyre and felsic norite in the upper 1500 m of the 3-D rock volume investigated by the combined 1998-99 surveys provides ideal conditions for the propagation of seismic waves with little scattering or attenuation and little variation in velocity until the target zones are reached. Modelling of this P- and S-wave first breaks showed velocity variations of 5830 to 6140 m/s for the P-waves from the 10 VSPs and 3410 to 3800 m/s for S-waves. The velocity between modeled diffractor and receiver was the most critical to the modeling so a velcoity value appropriate to each diffractor was chosen. In almost all cases a P-wave velocity of 6300 m/s and a S-wave velocity of 3600 m/s were used in the modeling.

At depths greater than 1500 m, the geological structures, rock units and ore deposits form complex structures at the margin between the igneous complex and the wall rocks to the impact crater. Numerous large breccia blocks, lenses and thickness variations of Sublayer norite provide numerous diffractor points and local reflectors. This combination of features provides VSP records very rich in clear signals that are useful only if they can be isolated.

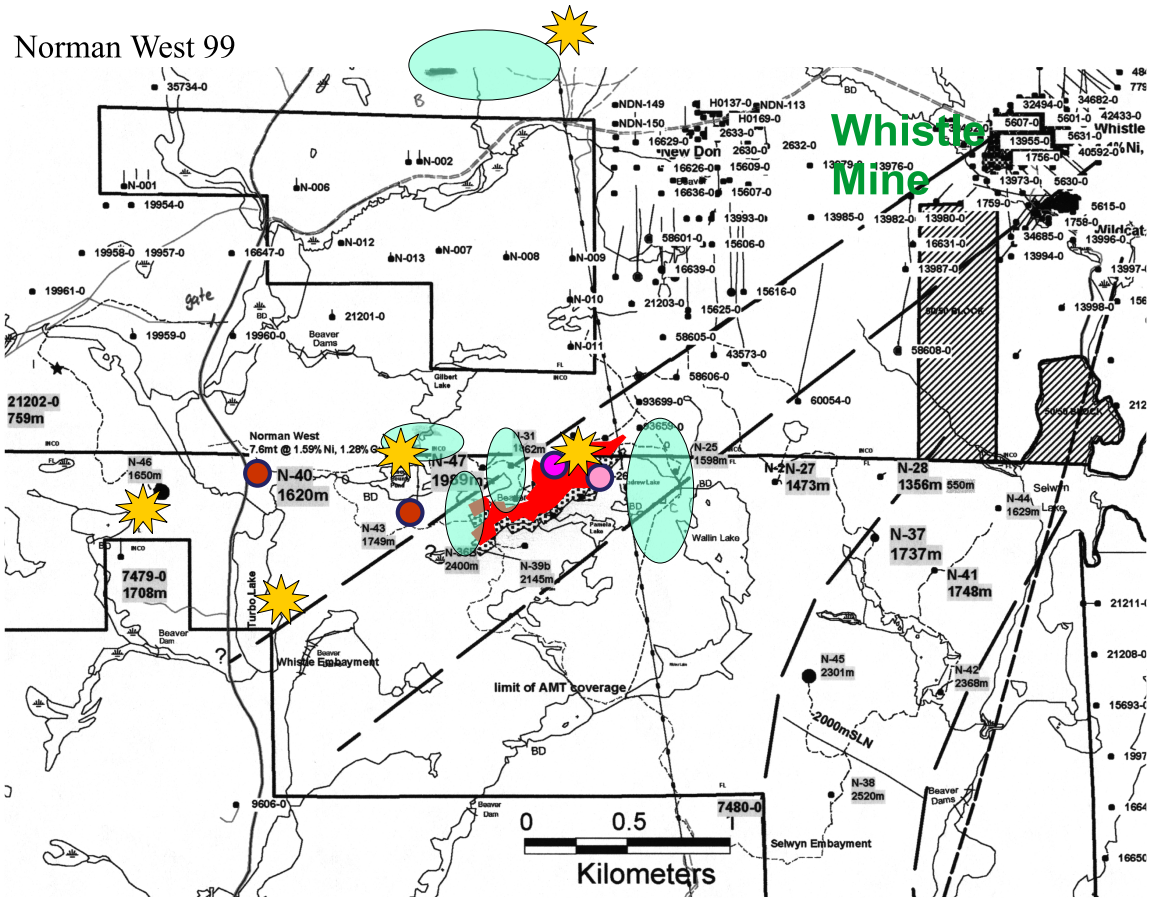

Figure 17.1: Location map for the 1999 Norman West survey. Red dots locate the receiver holes N-40 and N-43; the orange stars locate the five shot points used. Pink dots are the locations of the two holes used in 1998 (see below). The bright red object is the embayment ore deposit as identified by Falconbridge. The green ellipses are estimates of strong diffractor locations based on the current DSI survey results.

Interpretation Procedure

Modeling was done primarily by trial and error matching of travel times using synthetic travel time curves generated by DSIsoft code developed by Ian Kay (see curves on Figures 2-4). Amplitudes were not considered explicitly. Diffractors and reflecting planes, sources and receivers were assumed to lie within a rock volume of uniform velocity. In general, directions are accurate only to 20, depths to 50 m, offset estimates can vary by as much as 500 m. If a particular diffractor is isolated for further study, these uncertainties could be reduced by further modeling that incorporates amplitudes and 3-D particle motion.

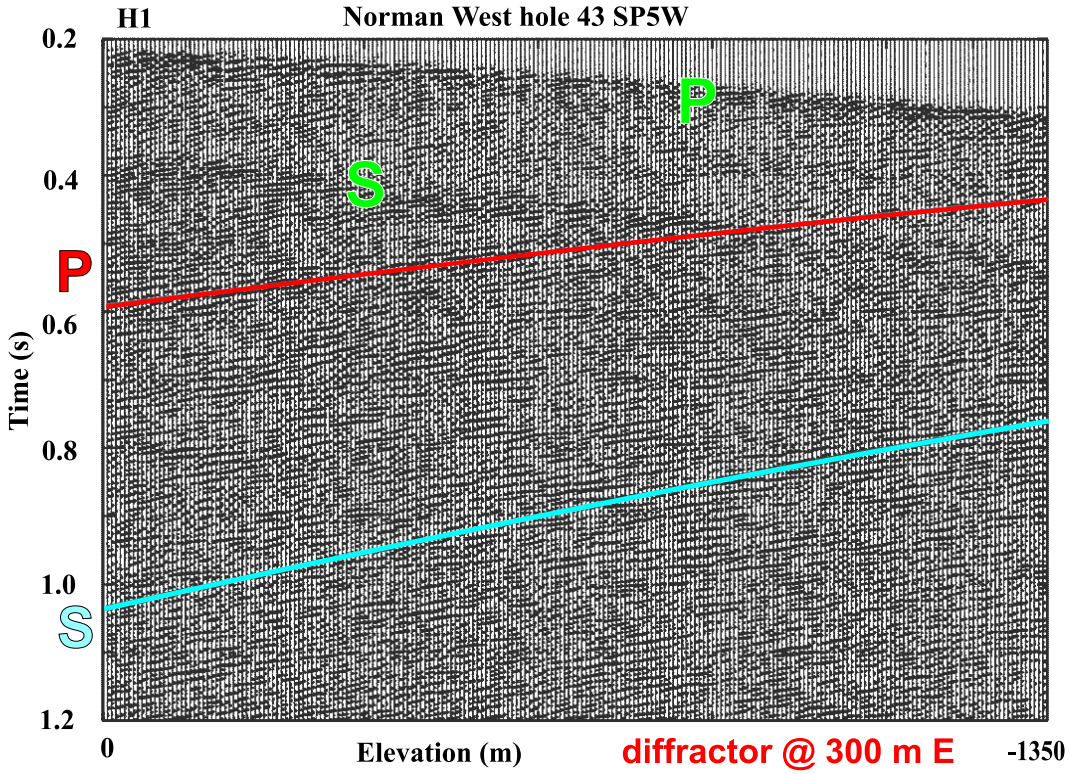

Figure 17.2: Time-offset plot for SP5W as recorded by the H1 component in hole N43. The colored curves indicate theoretical curves [I. Kay, DSIsoft code] for a single diffractor located 300 m east of N43 (see Table 1). The first curve (red) is modeled assuming the energy is scattered from the body as P-waves traveling at 6300 m/s, the second curve (blue) assumes S-waves velocities of 3600 m/s. The background section is the final processed version of the data. Residual energy from direct P- and S-wave arrivals are also indicated.

Because the 1999 survey had data with three largely balanced components, interpretation concentrated on diffractions. For modeling, diffractors were treated as local seismic sources and located spatially much as earthquakes would be located using five observatories. The apex or focus of each diffraction hyperbola observed on the record was assumed to mark the depth of the diffractor. Travel times were then matched from each shot point to a test diffractor location and the test location adjusted until a good fit was achieved.

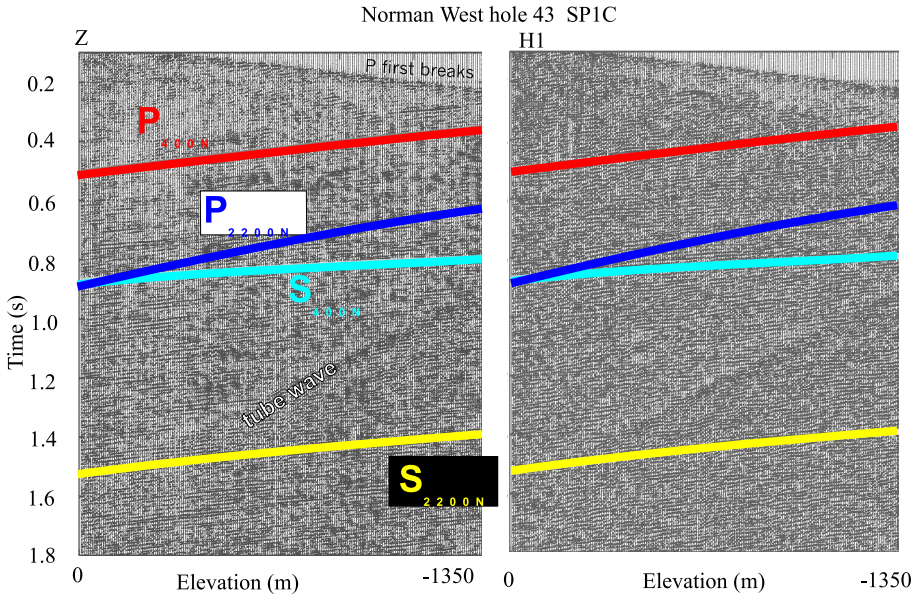

Figure 17.3: Time-offset plot for SP1C as recorded in hole N43 and comparing the vertical and radial horizontal components. The horizontal axis increases from the shallowest receiver point (trace interval is 5 m), so this plot shows wireline depths between 350 and 1705 m. The four colored curves indicate theoretical curves [I. Kay, DSIsoft code] for diffractors located at offsets of 400 m north (red and cyan) and 2200 m north from N43 royal blue and yellow (see Table 1). The first curve in each pair is modeled assuming the energy is scattered from the body as P-waves with 6300 m/s velocity, the second curve assumes S-wave velocities of 3600 m/s. The background section is the final processed version of the data. Residual energy from a tube wave and direct arrivals are indicated.

Emphasis was placed on the shape of the diffraction hyperbole. Most were best matched assuming S-wave velocities between diffractor and receiver. This is consistent with recent synthetic modeling done on model ore bodies by Richard Hobbs using the phase screen method where he showed that P-S conversions were the most efficient scattering mechanism. A few showed P- and S-wave travel times consistent with an origin at the same diffractor (Figures 2 and 3) which greatly increases confidence in the modeling. Only when travel times of prominent diffractors indicate consistent locations using six or more VSPs (source-receiver pairs) are they listed in the results (Table 1). Many more diffractors were considered and modeled.

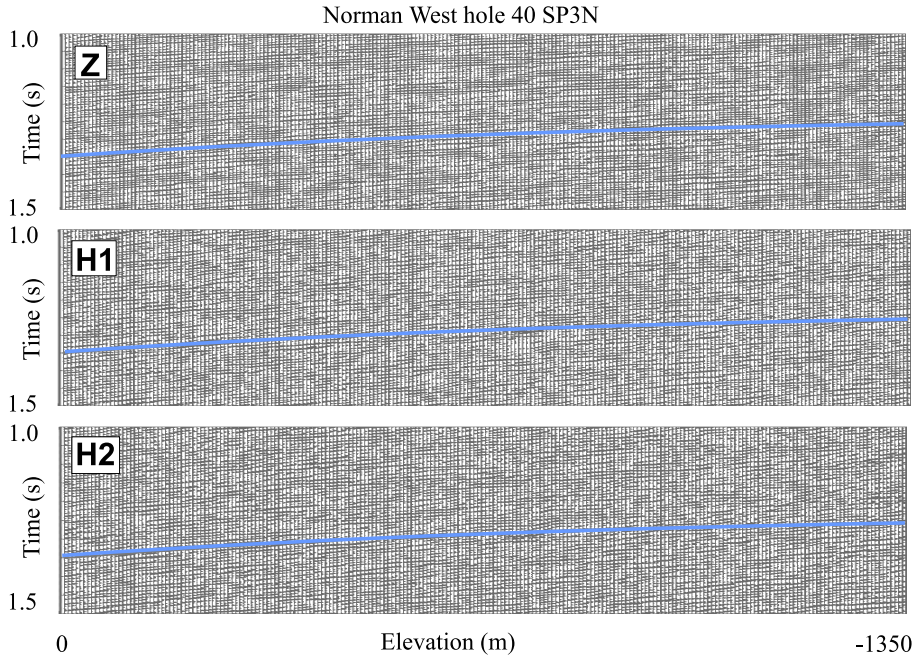

Figure 17.4: Time-offset plot for SP3N as recorded in hole N40 comparing all three components. Format as in other figures. The colored curves indicate theoretical curves [I. Kay, DSIsoft code] for a single diffractor located 1600 m east of N40 (see Table 1). The curve is modeled assuming the energy is scattered from the body as S-waves with velocities of 3600 m/s. The background section is the final processed version of the data.

Preliminary Interpretation of the Norman West 99 dataset

Five diffractors were modeled using most shot points and receivers in both holes N40 and N43 (Table 1, Figure 1). One of these (Figure 2) appears to coincide with diffractors previously identified using data from holes N26 and N33. Three lie around the margins of the known massive sulfide deposit associated with the Norman West deposit (Figure 1). Although specific local ore bodies may not yet have been resolved, clearly some of the most prominent diffractors originate where massive sulfide ore bodies are known from drilling or inferred from downhole EM surveys. We therefore feel that we have now successfully calibrated our VSP technique out to distances as great as 1500 m and arguably out to 2500 m (diffractor near N25 observed in N40). One new fault plane was modeled in addition to those identified with the 1998 data. It coincides with a prominent reflection that intersected hole N26 at -1272 m elevation (-1280 m in N33), strikes 330 and dips 25-30 W (Figure 1). It is interpreted as the lower contact of the Sublayer norite.

Hole	SP	component	offset(meters E,N,Z)	velocity (m/s)
N43	1C	Z,H1	0,400,0	6250, 3600
N43	3N	Z,H1,H2	0,400,0	3800
N43	4S	Z,H1	0,500,0	6400, 3400
N40	2E	Z	600,0,200	6300
N40	3N	Z	400,0,-200	6300
N40	5W	Z	950,0,-300	6300
N43	1C	Z,H1	0,2200,0	6250, 3600
N43	5W	Z	0,2200,0	3600
N43	5W	H2	0,1800,0	6300
N43	4S	Z,H1,H2	0,1800,0	3400
N40	1C	Z,H1	0,1850,0	6300
N40	2E	Z,H1	0,1000,0	3600
N40	2E	Z,H2	0,2000,700	3600
N40	4S	Z,H1	0,1400,0	3600
N40	5W	Z,H2	0,1800,600	6300
N40	5W	H2	0,1800,700	3500
N43	1C	H2	2000,0,300	3600
N43	2E	Z	2400,0,100	3600
N43	3N	H1	2000,0,500	3800
N40	1C	Z,H1	2700,0,900	3600
N40	2E	Z,H2	2700,0,900	3600
N40	3N	H2	2500,0,1000	3600
N43	2E	Z	300,0,0	6300
N43	5W	Z,H1	300,0,0	6300, 3600
N40	2E	Z,H1	800,0,0	6300
N40	4S	Z	1200,-300,0	3600
N40	1C	Z	1200,0,0	6300, 3600
N40	1C	Z,H1	1800,0,0	6300, 3600
N40	2E	Z	1500,0,0	3600
N40	3N	Z,H1,H2	1600,0,0	3600
N40	5W	Z,H2	1000,0,-200	6300
N403	1C	H2	670,0,200	3600

Table 17.1: Diffractors identified from the 1999 Norman West survey. NB Z is relative to bottom of hole (+ downward).

Chapter 18

Interpretation of the Norman West 99 data sets: CDP transform results

By **Gervais Perron**

Introduction

The survey designs used for the Norman West '98 and '99 have a built in imaging component. Each VSP defined by a shot point and a recording borehole can be mapped into an ordinary seismic profile assuming certain parameters. In the case of Norman West '99, some profiles run parallel one to each other forming a pseudo-3D volume of 4 km^2 with a maximum depth of more than 2.5 km. This cube contains the boundary between the ore bearing embayment structure and the barren footwall contact.
Data from the Norman West '98 data provide good control at the recording boreholes and direct correlations can be made between observed reflections and core samples. This is why one of last year's profile included in the volume is used here as a basis for interpreting some of this year's datasets.
Profiles derived from 3 VSPs recorded in borehole N-40 (shot points central, east and north) were chosen because of their long offsets and preferable position to image the main Sudbury Igenous Complex (SIC) lithologies.
In 1998, the Sublayer Norite contact with the Late Granite Breccia was mapped from its intersection with borehole N-33 to a distance of about 600 m to the north-east. This year, the same contact is interpreted on more than a kilometer based on data recorded more than 1.5 kilometer to the west (borehole N-40) along with a reflection believed to represent a footwall intrusion.

Theory

Although relatively easy to implement and to apply, the CDP Transform has limitations. Several basic assumptions must be taken into account. First, the velocity field is considered constant. In mineral applications this limitation is acceptable since in hard rocks, velocity variations are around than 15 percent. The second serious limitation is that the CDP Transform handles properly only data corresponding to a limited dip angle range. And finally, the reflecting object must be a planar surface. Curved interfaces and diffractors cannot be properly resolved using the CDP Transform.
Where velocity is constant, a unique location in space can be attributed for a given shot-receiver geometry and travel-time. So, for each sample of each trace of an offset VSP profile the position of a corresponding reflection point in space is computed by the CDP Transform. The 3-D earth is divided in small cubes called bins. Each reflection point computed by the CDP transform is placed in its appropriate bin in space, thus reconstructing an image giving the true sub-surface position of all the reflecting horizons with a predefine dip along the offset VSP profile (Fig.18.2).
Given its limitations, the CDP Transform process is still a useful way to image certain events identified on offset VSP profiles acquired in hard rock environment. Marker horizons and fracture zones in mining camps can be imaged if information

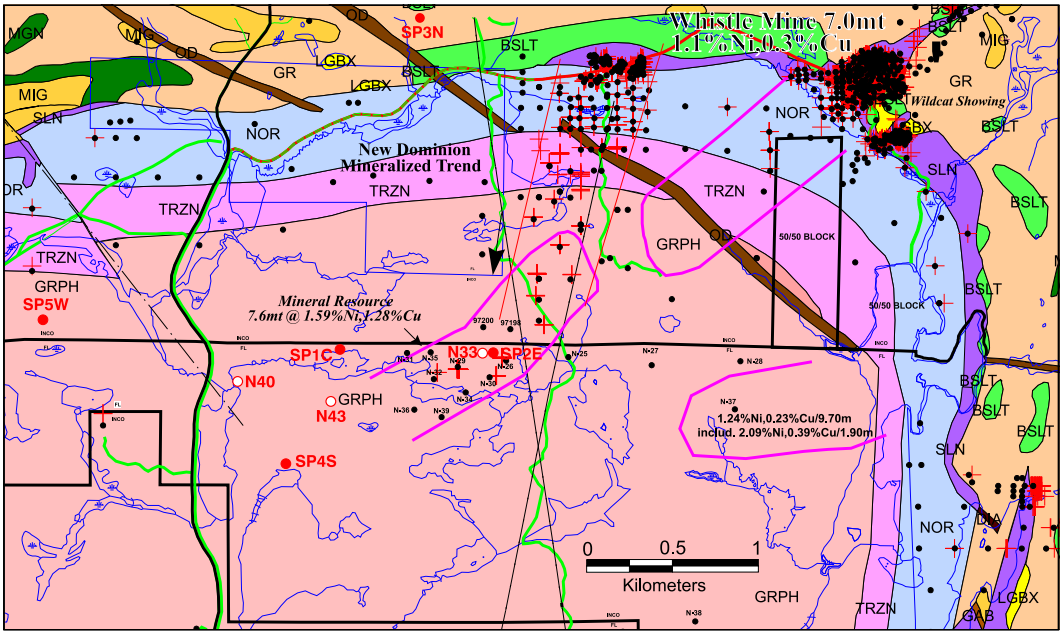

Figure 18.1: Norman West regional geology showing the SIC units, mineral occurences and drillholes. The NW99 survey geometry is indicated in red and includes 5 shot points, 2 recording boreholes (N-40 and N-43) and the N-33 the borehole in which geophysical data were collected

about the strike and dip is known (generally derived from forward modeling of multi-offset/azimuth surveys). Other reflecting events like fracture zones can easily be mapped using this technique.

The '99 longer offset VSPs brought a new dimension to the data interpretation. With longer source-receiver offsets and updip shot position, the interpretation tip stating that "every reflection intersecting the first break arrivals must intersect the borehole at the depth where the first breaks were recorded" is no longer valid. In the case of the shorter offsets we assume that the reflection points are located close to the borehole. This assumption is no longer valid when confronted with longer offsets and an updip shot point location. An alternate interpretation puts the reflection points underneath the source point. Figure 18.3 shows the case of shot point 3 north and recording borehole N-43 where a reflection from a plane striking N 150 degree and dipping 30 degrees is intersecting the first breaks at a depth of 1115 m. The associated reflection points are shown in figure 18.4. Note that none of the CDP points is intersecting the recording borehole, as a matter a fact they are located close to the source point. This is a potential interpretation pitfall associated with a long offset survey design. The interpreter who is not using the CDP Transform mapping process, which is an unbiased representation, may come to the wrong conclusions.

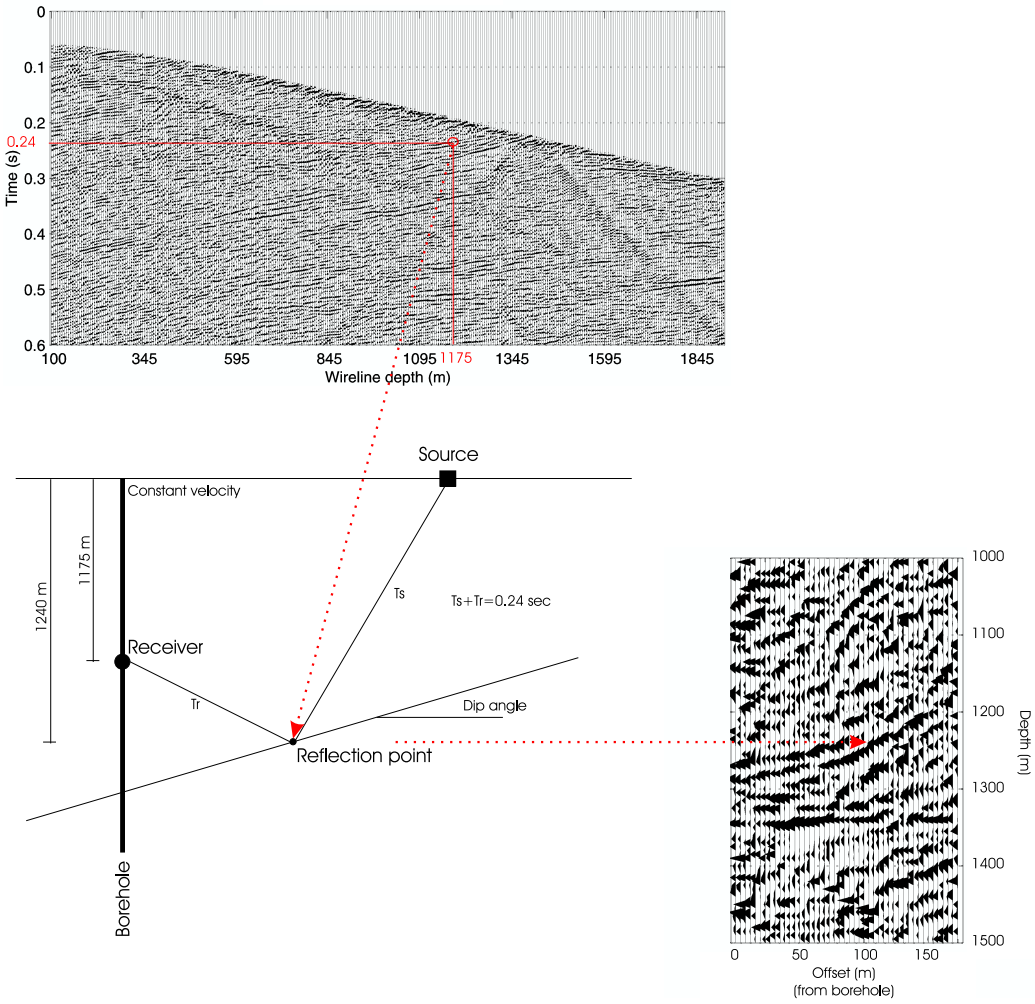

Figure 18.2: Cartoon of the CDP Transform process.

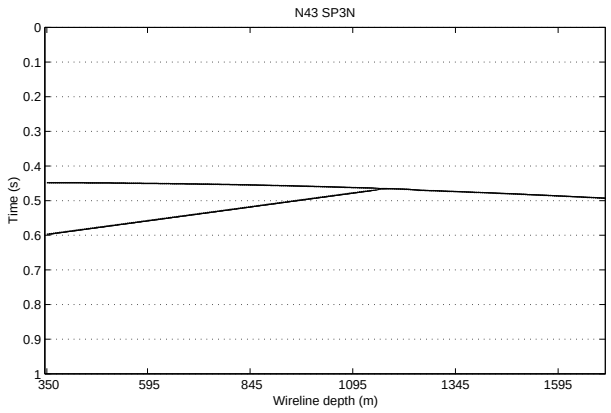

Figure 18.3: Synthetic dataset of a plane striking at N 150 degrees and dipping 20 degrees from a VSP profile shot at the North shot point and recorded in hole N-43. The reflection is intersecting the first break arrivals at a depth on 1115 m.

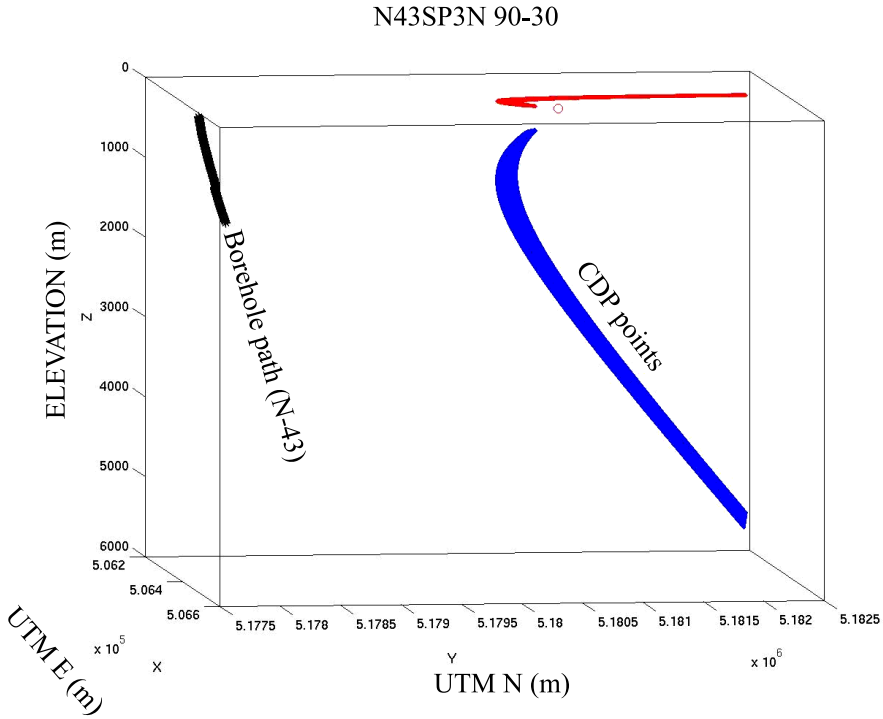

Figure 18.4: Reflections points associated with the reflection shown in Fig.18.3. Note that non of the reflection points are intersecting the recording borehole even though the reflection is intersecting the first break arrivals.

Velocity Analysis

In order to properly constrain the CDP Transform mapping process, it is important to have a good knowledge of the average background P-wave velocity of the SIC units. This can be achieved by analyzing first break arrival times from a zero (or short) offset VSP survey. A linear regression through the first break times provides a robust estimate of the average background velocity and shot statics. First break arrivals were picked on data recorded from N-43 and fired at the central shot point. The regression was done on 272 picks from offsets ranging between 400 and 1600 m. The inverse of the slope yielded an average velocity of 6300 m/s with a shot static of 27 ms (Fig.18.5). This estimate is in good agreement with sonic data collected in borehole N-33 and measurements made on mini-cores under a pressure of 200 MPa and will be used for the CDP Transform processing.

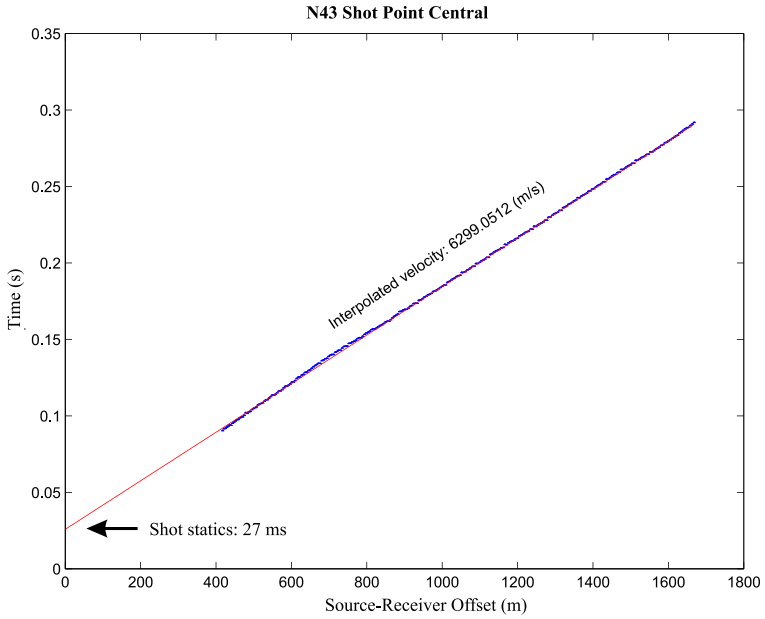

Figure 18.5: Linear regression results on first break arrival times from N-43 and shot point central. An average velocity of 6300 m/s was computed and associated shot statics were estimated at 27 ms.

Procedure for interpreting CDP Transform profiles

By combining results from both the '98 and '99 datasets, we can take advantage at the fact that some of the 1998 CDP Transform profiles intersect exploration drillholes (N-26 and N-33). Thus, interpretation of reflections associated with lithological contacts

that intersect a borehole is done unambiguously. This will be the starting point of this interpretation.

Four CDP Transform profiles were selected for this interpretation based on their susceptibility to image the known units of the SIC and more particularly the Sublayer Norite/Late Granite Breccia contact. They are N40sp1C, N40sp2E, N40sp3N and N33sp4. Those profiles identified by their respective source point and recording borehole all have midpoints aligned perpendicular to the known strike azimuth of the SIC units (N 150 degrees). They are more prone to image the true dip of the units evaluated at 30 degrees for the exercise. Borehole N-40, located further away (more than 1.5 km) from the Norman West embayment, was preferred to N-43 to demonstrate that the CDP Transform procedure is able to image lithological contacts from such great distances.

Figure 18.6 shows the distribution of the midpoints from each CDP Transform profile. The binning line for each profile runs between the corresponding gray squares. In the case of N33sp4 (blue midpoints) the midpoints intersect the borehole (N-33). The limits of the reflection associated with the Sublayer Norite on that profile start at the borehole (red circle over borehole N-33) at a depth of 1500 m and is traced updip more than 800 m away from the borehole (second red circle) to a depth of 1200 m. This reflector was imaged unambiguously along the blue CDP points between both cyan lines.

The other red circles over the other CDP points (black, magenta and red) represents the intersection of the Sublayer Norite with the other CDP Transform profiles assuming that its strike azimuth is N 150 degrees.

The next step in the interpretation process is to track this lithological contact onto the other CDP Transform profiles and verifying if there is a reflector corresponding to that projected position in 3D space. The identical procedure was done for an interpreted footwall intrusion on the N33sp4 profile.

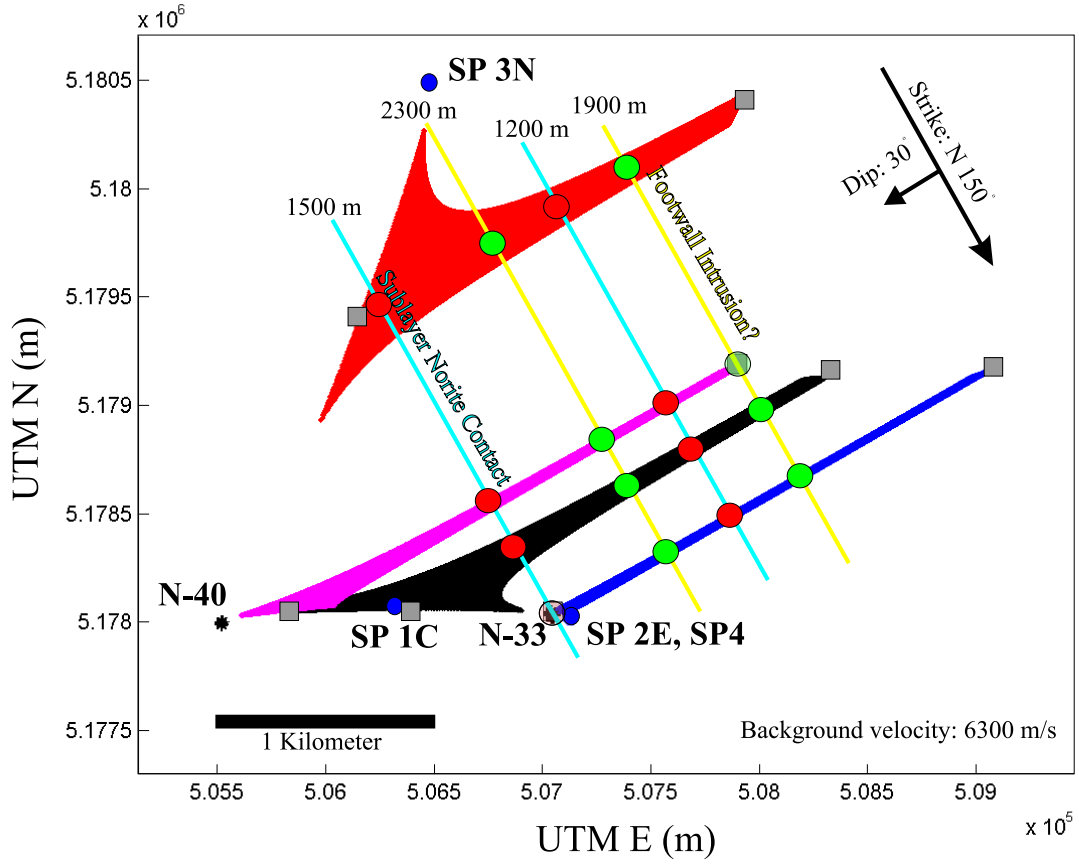

Figure 18.6: Plan view of the Norman West experiments. Surface projection of the reflection points for n33sp4, n40sp2e, n40sp1c and n40sp3n are respectively shown in blue, black, magenta and red. Red and green circles define the limits of the SLN contact and footwall intrusion. The cyan and yellow lines represent the depth contours of these units.

Interpretation Results

The Sublayer Norite (SLN) contact intersects borehole N-33 at approximately 1500 m depth as noted in the geological logs from Falconbridge. Figure 18.7 shows the interpreted SLN highlighted in cyan (bounded by red circles). Its start point intersects the borehole at 1500 m depth and is traced updip to a depth of 1200 m. These are the control points of the interpretation. A footwall intrusion (maybe a gabbro) is identified the same way (yellow, bounded by green circles).

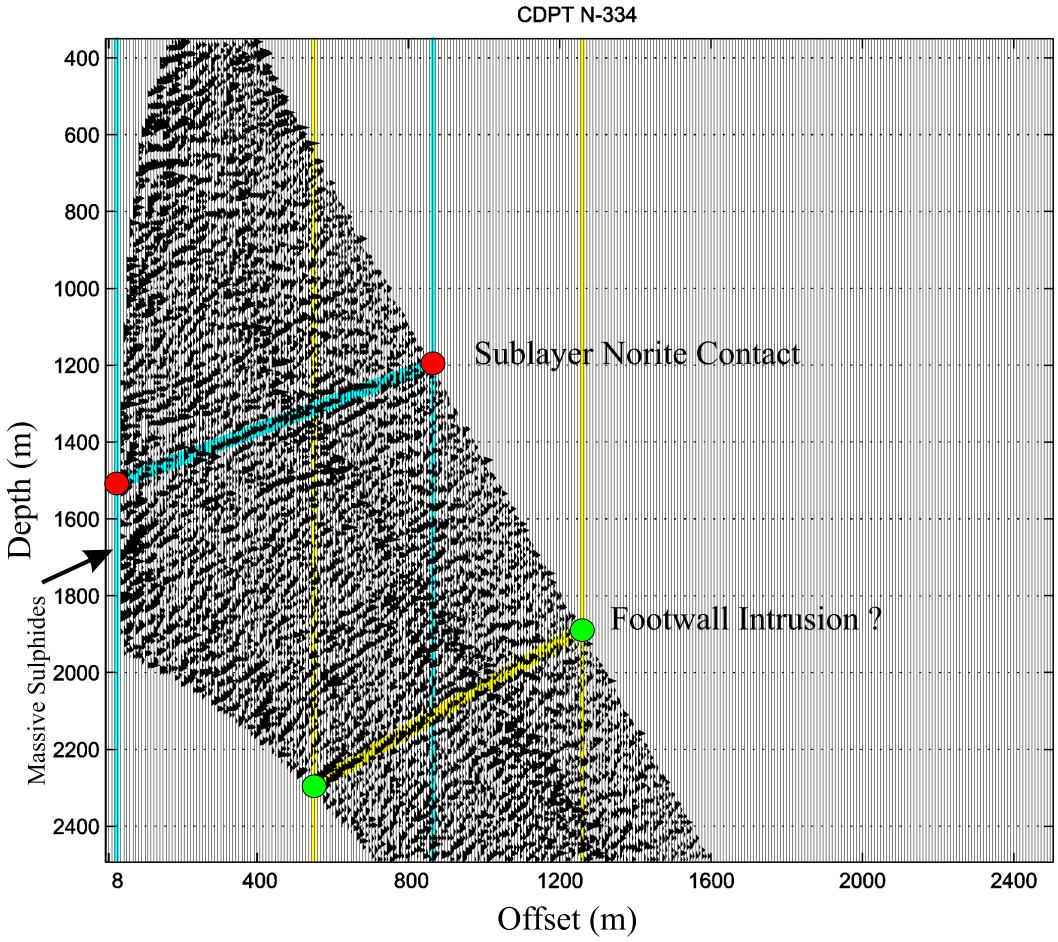

Figure 18.7: CDP Transform profile from N33sp4 corresponding to the blue profile. The SLN contact is identified at the borehole intersection making the interpretation unambiguous. Note the response from the massive sulphide intersection (arrow).

These circles can be projected at the surface as seen on figure 18.6. The idea is then to project those circles laterally along a N 150 degrees azimuth on the other CDP Transform profiles (black, magenta, red). This is done arbitrarily without any reference to the seismic data. This means that the interpreter has no control on where those points will fall on the other profiles. Once the position of those circles are identified on each profile, they can be projected down at their respective depths (1500 and 1200 m for the SLN and 2300 and 1900 m for the footwall intrusion). Then it is possible to see if any reflection is correlating with the theoretical position of the SLN or footwall intrusion on each CDP Transform profiles.

Note the prominent reflection along the borehole at a depth of 1700 m. Figure 18.8 a blowup section around the ore zone intersection. The ore reflection can be traced on 7 traces (48 meters) before abruptly disappear. A preliminary interpretation of this reflection suggests that the extension of the ore lens to the north-east is of limited length (less than 100 m). This clear image of the ore zone is a direct result of the new implementation of the 3D CDP Transform algorithm. This new version coded by Gilles Bellefleur gives a better resolution in low fold areas close to the borehole. No real diffraction is visible on the section probably due to its weak amplitude on the VSP profile. Further studies should be done on reflections directly linked with ore bodies identified on the Norman West datasets.

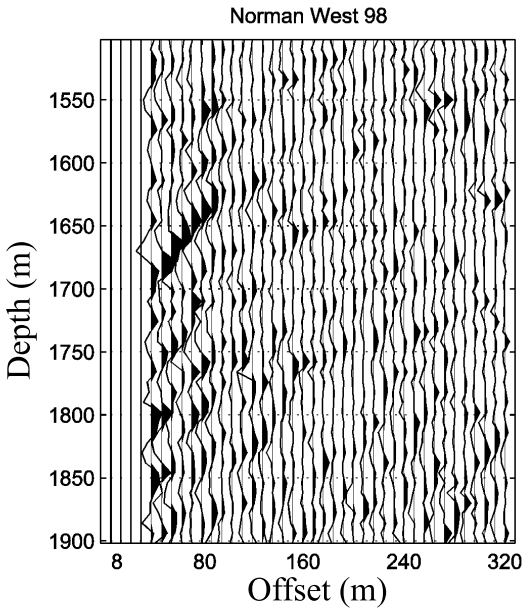

Figure 18.8: CDP Transform image of the ore zone intersected by borehole N-33. The ore has been imaged on 48 m away from the borehole N-33 towards the north-east direction. No diffraction signature is visible on the profile probably due to its weak amplitude on the original VSP profile.

The projection of the SLN contact and footwall intrusion limits on the profile defined by shot point 2E and borehole N-40 is done laterally along strike (N 150 degrees). The red and green circles are moved onto the black profile (Fig.18.6). Figure 18.9 shows the theoretical position of both contacts on the black profile (thick cyan and yellow lines). A prominent reflection coincides with this he SLN position. The reflection associated with the footwall intrusion shows some curvature inferring that this feature is probably not totally concordant with the SIC units. Both contacts were successfully mapped more that 400 m north-west of borehole N-33.

A second projection on the magenta profile defined by shot point 1C and borehole N-40 was done. The SLN image at depth corresponds well with the strongest reflection on the profile (cyan) while the footwall intrusion lines up with a series of broken reflectors (Fig.18.10). Again, this demonstrate that this technique can map lithological contacts more than 625 m away from N-33 and 2400 m from N-40.

The final test was to project the SLN and footwall intrusion on a distant profile defined by shot point 3N and borehole N-40 (red). This profile is located more than 1.5 km along strike from the original blue profile. Analysis of the data shows that the predicted position of the SLN contact (cyan) is about 50 m below a major reflection on the profile (Fig.18.11). We believe that this reflector is associated with the SLN for the following reason. Since the Norman West property is located in the north-east corner of the Sudbury Structure the main SIC units tends to change azimuth from N 150 degrees towards N 90 degrees above shot point 3N (Fig.18.1). This has for effect to bring the SLN contact closer to borehole N-40 effectively bringing the contact shallower. Even though this explanation is physically possible, there might be alternate causes for this 50 m shift in the data. As for the footwall intrusion, it can no longer be associated with a reflector. It is believed that the lateral extent of this unit is localized compare to the SIC units and did not reached the distant n40sp3n CDP Transform profile.

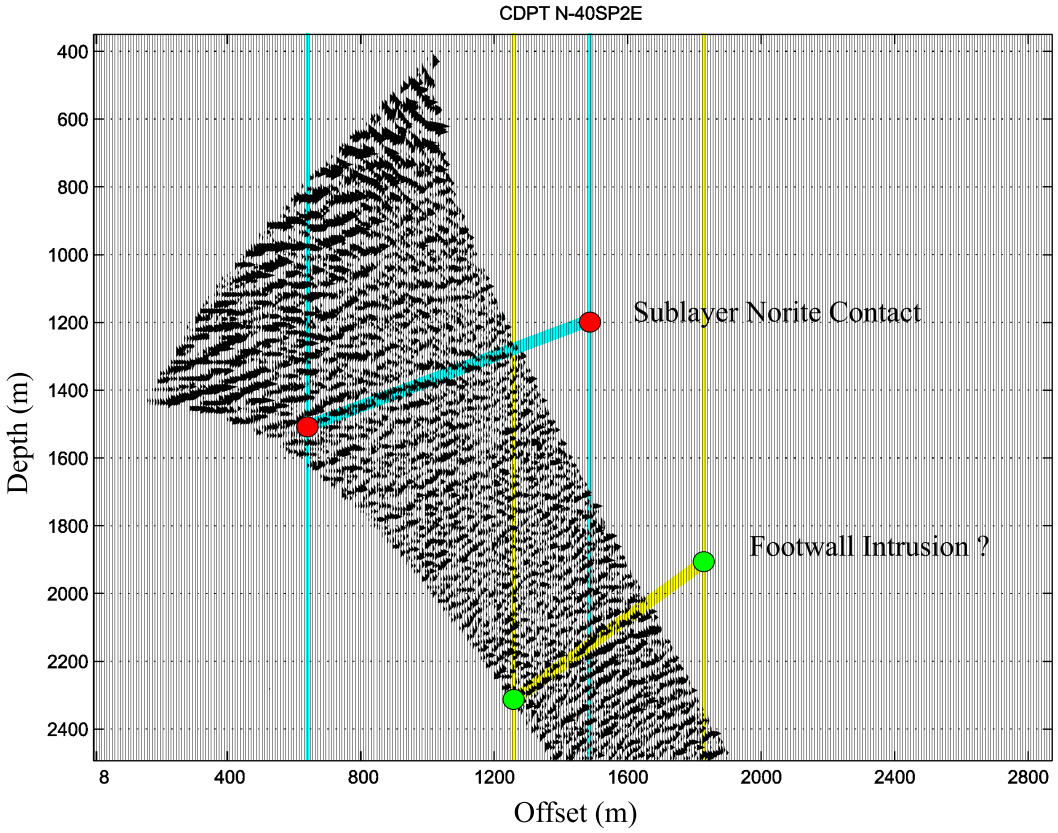

Figure 18.9: CDP Transform profile from n40sp2e (black profile). There is a good correlation between the predicted SLN position and a major 30 degrees dipping reflector. The deviation of the reflector associated with the footwall intrusion can be attributed to the fact that the intrusion is probably not always concordant with the SIC units.

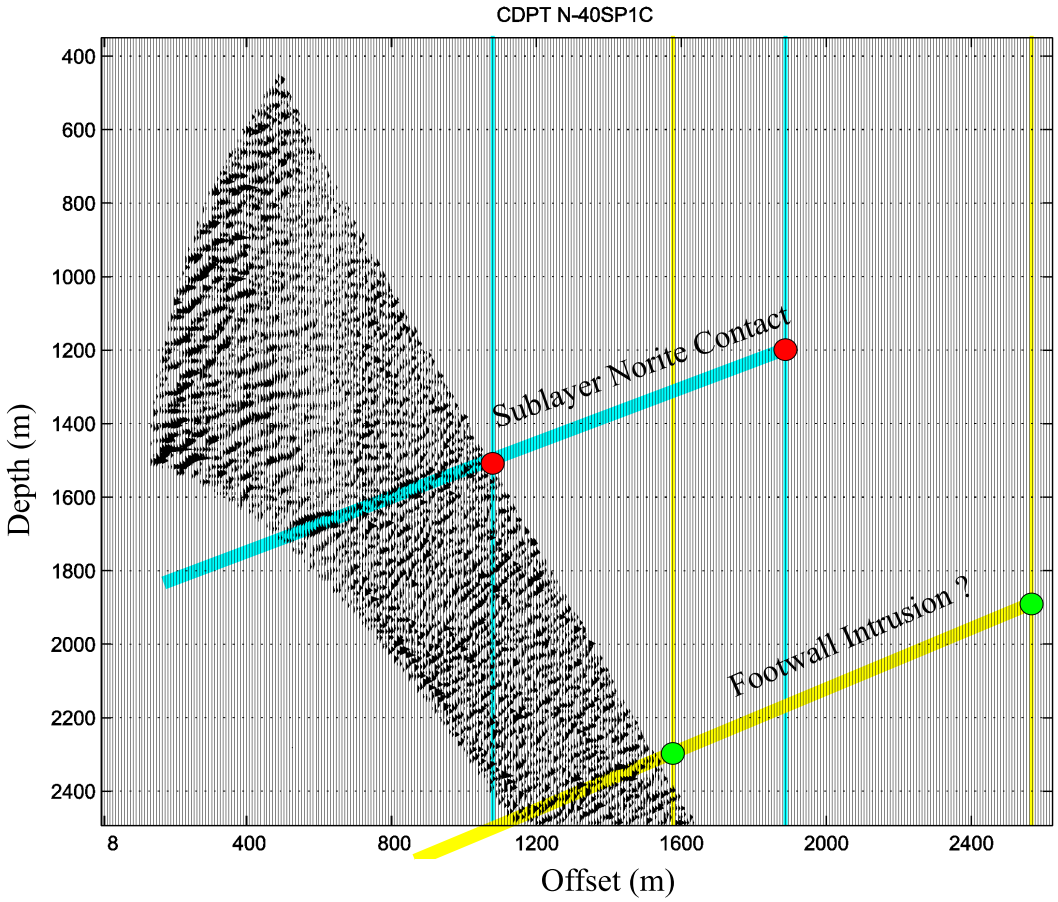

Figure 18.10: CDP Transform profile from n40sp1c (magenta profile). The predisted SLN contact position corresponds with the strongest reflector in this section. The footwall intrusion can be associated with a series of broken up reflectors.

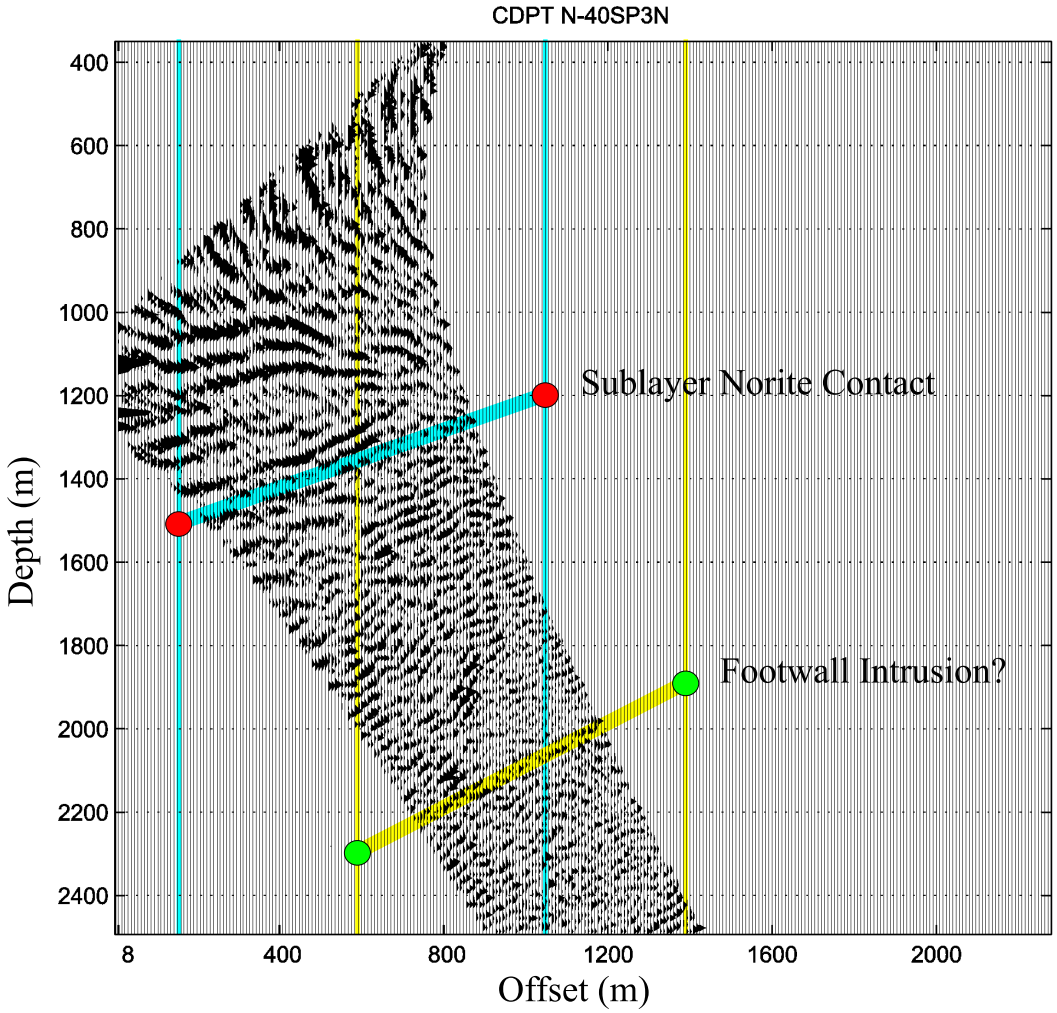

Figure 18.11: CDP Transform profile from n40sp3n (red profile). Distortion above the 1000 m mark is due to the extensive scattering of the reflection points. The 50 m misfit in the data can be attributed the the fact that the SIC units are gradually changing azimuth in the north-east corner of the Sudbury Structure bringing the SLN contact closer and shallower than estimated by the CDP Transform process (cyan). There is no longer a reflector associated with the footwall intrusion. This is probably because the intrusion has a limited lateral extension that did not reach the red profile.

Conclusions and recommendations

This simple interpretation process was able to show that the lateral extension of the SIC units and footwall features can be mapped on a 4 km^2 grid to a depth of 1500 m using two boreholes and three shot points. Data from N-40 was recorded more than 1 km away from the Sublayer Norite contact it images.
This interpretation could be expanded to include all the available datasets from N-40, N-43, N-33 and N-26. It is important to use a dataset containing reflection points that intersect the recording borehole as a starting point for the interpretation. That is why it is important to record at least one shot offset VSP dataset.

Chapter 19

List of participants

Erick Adam
GSC/CGD
212-615 Booth Street
Ottawa, Ontario K1A 0E9
Canada
Business: (613) 947-1579
Business Fax: (613) 943-9285
E-mail: eadam@NRCan.gc.ca

Gilles Bellefleur
Dept. C.G.M.
Ecole Polytechnique
Montreal, Québec H3C 3A7
Canada
Business: (514) 340-4711 x5233
Business Fax: (514) 940-3970
E-mail: belfleur@geo.polymtl.ca

Thomas Bohlen
Christian-Albrechts-Universität zu Kiel
Institut für Geowissenschaften
Abteilung Geophysik
Otto-Hahn-Platz 1
24118 Kiel, Germany
Business: (+49) 431-880-4648
E-mail: tbohlen@physik.uni-kiel.de

Robert Burns
GSC/TSD
186-601 Booth Street
Ottawa, Ontario K1A 0E8
Canada
Business: (613) 992-2886
Business Fax: (613) 992-0190
E-mail: burns@NRCan.gc.ca

Greg Clarke
Dept. of Earth Sciences
University of Western Ontario
London, Ontario N6A 5B7
Canada
E-mail: gclarke@seis.gp.uwo.ca

Marten Douma
GSC/TSD
185-601 Booth Street
Ottawa, Ontario K1A 0E8
Canada
Business: (613) 992-0341
Business Fax: (613) 992-0190
E-mail: mdouma@NRCan.gc.ca

Eric Duveneck
Christian-Albrechts-Universität zu Kiel
Institut für Geowissenschaften
Abteilung Geophysik
Otto-Hahn-Platz 1
24118 Kiel, Germany
Business: (+49) 431-880-4648
E-mail: eric@geophysik.uni-kiel.de

David Eaton
Dept. of Earth Sciences
University of Western Ontario
London, Ontario N6A 5B7
Canada
Business: (519) 661-3190
Business Fax: (519) 661-3198
E-mail: deaton@julian.uwo.ca

J. Hawken
Dept. of Earth Sciences
Dalhousie University
Halifax, NS B3H 4J1
Canada

Richard Hobbs
Bullard Laboratories
Madingly Road
CB3 0EZ
UK
Business: +44 (1223) 337060
Business Fax: +44 (1223) 360779
E-mail: hobbs@esc.cam.ac.uk

Jim Hunter
GSC/TSD
182A-601 Booth Street
Ottawa, Ontario K1A 0E8
Canada
Business: (613) 992-2560
Business Fax: (613) 992-0190
E-mail: jhunter@NRCan.gc.ca

Marko Mah
University of Alberta
Department of Physics
Edmonton, Alberta T6G 2J1
Canada
Business: (780) 492-3985
E-mail: mah@phys.ualberta.ca

Bernd Milkereit
Christian-Albrechts-Universität zu Kiel
Institut für Geowissenschaften
Abteilung Geophysik
Otto-Hahn-Platz 1
24118 Kiel, Germany
Business: (+49) 431-880-3914
Business Fax: (+49) 431-880-4432
E-mail: bmilkereit@geophysik.uni-kiel.de

Christof Müller
Christian-Albrechts-Universität zu Kiel
Institut für Geowissenschaften
Abteilung Geophysik
Otto-Hahn-Platz 1
24118 Kiel, Germany
Business: (+49) 431-880-4648
E-mail: cmu@geophysik.uni-kiel.de

Jonathan Mwenifumbo
GSC/MRD
575-601 Booth Street
Ottawa, Ontario K1A 0E8
Canada

Business: (613) 992-6520
Business Fax: (613) 996-3726
E-mail: jarako@NRCan.gc.ca

Carla Osborne
University of Alberta
Department of Physics
Edmonton, Alberta T6G 2J1
Canada
E-mail: osborne@phys.ualberta.ca

Gervais Perron
GSC/CGD
615 Booth Street
Ottawa, Ontario K1A 0E9
Canada
Business: (613) 996-2400
Business Fax: (613) 943-9285
E-mail: perron@cg.NRCan.gc.ca

Karen Pflug
GSC/MRD
583-601 Booth Street
Ottawa, Ontario K1A 0E8
Canada
Business: (613) 992-1083
Business Fax: (613) 996-3726
E-mail: kpflug@NRCan.gc.ca

Brian Roberts
GSC/CGD
209-615 Booth Street
Ottawa, Ontario K1A 0E9
Canada
Business: (613) 992-5179
Business Fax: (613) 943-9285
E-mail: broberts@NRCan.gc.ca

Matt Salisbury
Bedford Institute of Oceanography
P.O. Box 1006
Dartmouth, Nova Scotia B2Y 4A2

Canada
Business: (902) 426-2002
Business Fax: (902) 426-1466
E-mail: msalisbu@NRCan.gc.ca

Douglas Schmitt
University of Alberta
Department of Physics
Edmonton, Alberta T6G 2J1
Canada
Business: (780) 492-3985
E-mail: doug@phys.ualberta.ca

David Snyder
GSC/CGD
615 Booth Street, Rm. 204
Ottawa, ON
Canada K1A 0E9
Telephone: (613) 992-9240
Fax: (613) 943-9285
E-mail: dsnyder@NRCan.gc.ca

Robert Zschuppe
University of Waterloo
Business: (519)888-4567 x5023
E-mail: zschuppe@canada.com